



Peer review status:

This is a non-peer-reviewed preprint submitted to EarthArXiv.

1 **On the seasonal predictability of the 2020 North Atlantic tropical cyclone**  
2 **season**

3 E. L. Levin<sup>a</sup> M. Chien,<sup>b</sup> E. A. Barnes,<sup>b,c</sup> H. He,<sup>d</sup> G. A. Vecchi,<sup>d,e</sup> W. Yang,<sup>e</sup>

4 <sup>a</sup> *Program in Atmospheric and Oceanic Sciences, Princeton University*

5 <sup>b</sup> *Faculty of Computing and Data Sciences, Boston University*

6 <sup>c</sup> *Department of Earth and Environment, Boston University*

7 <sup>d</sup> *High Meadows Environmental Institute, Princeton University*

8 <sup>e</sup> *Department of Geosciences, Princeton University*

9 *Corresponding author:* Emma Levin, [emma.levin@princeton.edu](mailto:emma.levin@princeton.edu)

10 ABSTRACT: The 2020 Atlantic tropical cyclone (TC) season was exceptionally active, producing  
11 over twenty named storms, yet several seasonal forecasts failed to predict such extreme activity  
12 across their ensemble spread. Even when forced with the observed 2020 sea surface temperatures  
13 (SSTs), physics-based models simulated only a moderately active season across their ensemble  
14 members. Using observations and statistical, dynamical, and deep learning (DL) models, we  
15 evaluate several hypothesis regarding why the observed hyperactive outcome fell outside the  
16 ensemble range of the physics-based models forced with observed SSTs. Analysis of observed  
17 large-scale conditions indicates that 2020 did not exhibit favorable predictors of hyperactivity,  
18 indicating that the moderate activity in the models should not be unexpected. We also find  
19 support for a role in subseasonal atmospheric variability in enhancing the 2020 activity relative  
20 to predictions based on monthly and seasonal characteristics. To comprehensively characterize  
21 the range of outcomes for the 2020 season, we construct a 1,000-member ensemble using an DL  
22 emulator forced with observed SSTs. The observed hyperactivity corresponds to a 0.5 percent event  
23 within this ensemble. Although highly unlikely in any single year, such an outcome has roughly a 20  
24 percent chance of occurring at least once in a 45-year period. Taken together, our findings support  
25 the interpretation that 2020 represents an unlikely but possible outcome, potentially enhanced  
26 by subseasonal atmospheric variability, given current understanding, models, and observations.  
27 These results serve to remind us that rare events will occur in a chaotic climate system, and large  
28 ensembles are one approach to sample them.

29 SIGNIFICANCE STATEMENT: The 2020 Atlantic tropical cyclone (TC) season was exception-  
30 ally active, producing more than twenty named storms, including Hurricanes Laura and Sally,  
31 which caused severe impacts. Yet several state-of-the-art weather and climate models, spanning  
32 both physics-based and deep learning (DL) approaches, failed to anticipate this heightened activity.  
33 Our study evaluates several hypotheses to explain the models' inability to realistically simulate the  
34 2020 season as hyperactive. Our findings indicate that the 2020 season was an unlikely outcome  
35 given the large-scale environmental conditions observed that year, rather than a fundamental failure  
36 by the modeling or observational systems used to study TCs. We use a novel approach of simulating  
37 1,000 possible 2020 scenarios with a DL-based model to quantify just how unlikely this event was.

## 38 1. Introduction

39 Tropical cyclones (TCs) that form in the North Atlantic Ocean pose severe hazards to communities  
40 across the United States and the Caribbean (Young and Hsiang 2024; Weinkle et al. 2018; Klotzbach  
41 et al. 2018; Pielke et al. 2008). Accurate forecasts are therefore essential for preparedness and  
42 risk mitigation. Short-term weather forecasts, issued several days in advance, provide critical  
43 guidance for evacuation decisions and emergency response. In contrast, seasonal forecasts, issued  
44 months before the onset of the hurricane season, aim to anticipate the overall characteristics of the  
45 upcoming season.

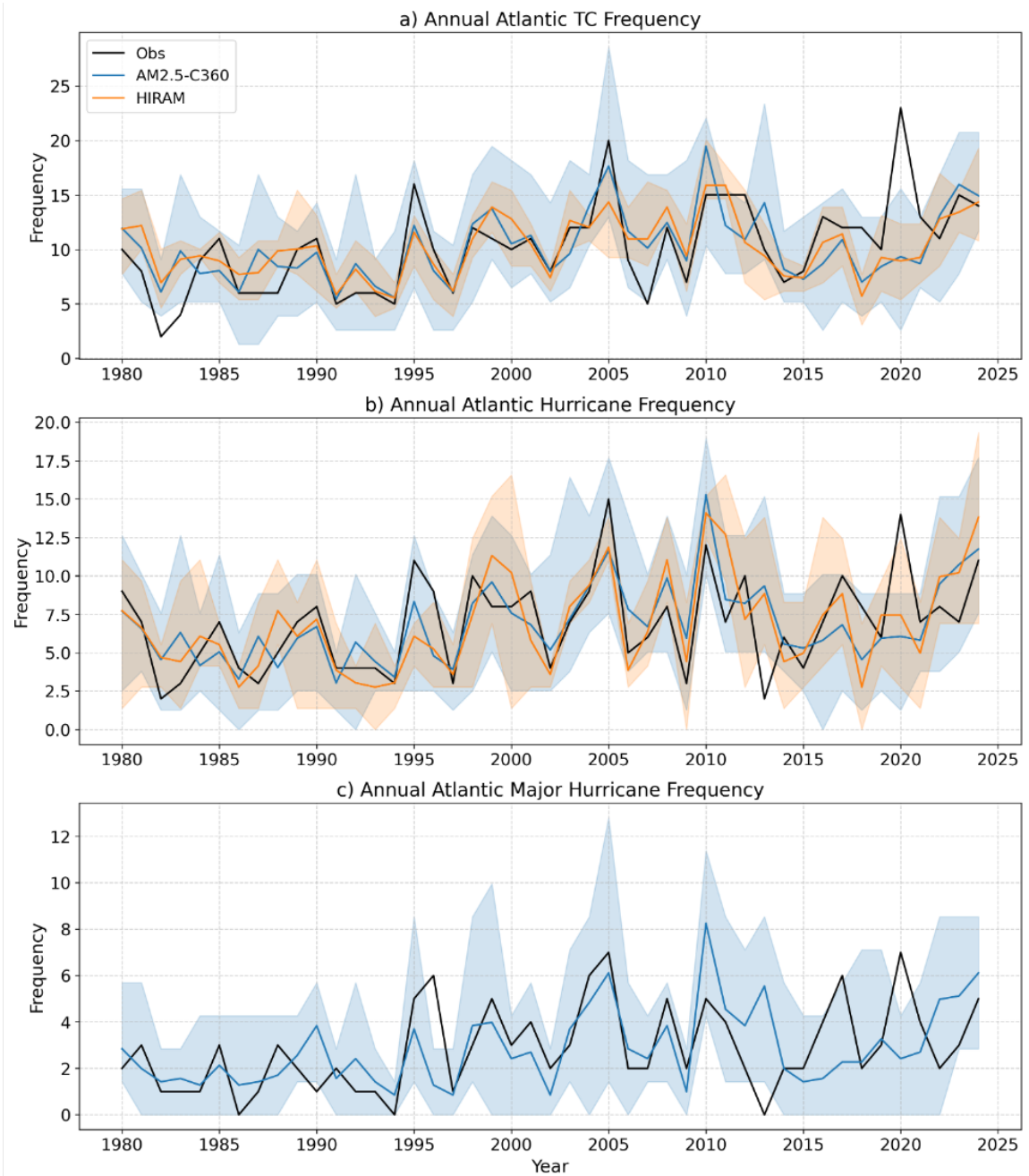
46 Seasonal forecasts can be generated by extending pre-season climate anomalies through the  
47 forecast period using dynamical models (e.g., Murakami et al. 2025; Vecchi et al. 2014; Vitart and  
48 Stockdale 2001; Zhao et al. 2010), statistical models (e.g., Gray 1984; Klotzbach and Gray 2003),  
49 hybrid statistical-dynamical models (e.g., Vecchi et al. 2011) or deep learning (DL)-based models  
50 (e.g., Zhang et al. 2025a). In addition, retrospective analyses can be performed to investigate  
51 the relationship between large-scale environmental conditions and past TC activity. This can be  
52 achieved using atmosphere-only dynamical models forced with observed monthly or daily historical  
53 sea surface temperatures (SSTs) (Delworth et al. 2012; Zhao and Held 2010; Zhao et al. 2009; Chen  
54 and Lin 2011) or statistical-dynamical models with observed monthly SSTs as predictors (e.g.,  
55 Vecchi et al. 2011). While these experiments do not reproduce the specific storms that occurred,  
56 they enable the generation of plausible realizations of past seasons and provide insight into the  
57 factors that contributed to periods of enhanced or reduced activity.

58 Evaluated over the extended period 1871-2024, two atmosphere-only models developed at the  
59 Geophysical Fluid Dynamics Laboratory (GFDL), HIRAM and AM2.5-C360, have demonstrated  
60 considerable skill in simulating both interannual and multidecadal variability of Atlantic TC  
61 activity when forced with observed monthly SSTs (Levin et al. 2025). Nonetheless, as expected for  
62 storm-season simulations (Vecchi and Villarini 2014), these models exhibit biases in certain years.

63 Since 1980, both models have generally captured the observed interannual variability in Atlantic  
64 TC counts, yet they verified poorly against the exceptionally active 2020 season. As shown in  
65 Fig. 1a, between 1980 and 2024, the observed storm counts computed using the methodology  
66 and duration thresholds of Landsea et al. (2010) typically fall within the ensemble spread of both  
67 models. The 2020 season represents a striking exception: while the models simulated a relatively  
68 moderate number of storms, with the ensemble means of both models anticipating roughly 8 storms,  
69 23 were observed. The observed activity in 2020 also lay at the extreme upper tail of the ensemble  
70 distributions from several coupled seasonal prediction systems (e.g., Murakami et al. 2025) and  
71 from a DL-based seasonal forecast (Zhang et al. 2025a). As shown in Fig. 1b and c, the ensemble  
72 spread poorly represents the 2020 storm count for more intense storms, including hurricanes and  
73 major hurricanes. Although the 2020 season's activity was remarkable, such hyperactivity is not  
74 without precedent. For instance, the 2005 Atlantic hurricane season produced 20 named storms,  
75 15 hurricanes, and 7 major hurricanes (Fig. 1). In that case, however, the observed TC, hurricane,  
76 and major hurricane counts fell within the ensemble range of the AM2.5-C360 model, and HIRAM  
77 also simulated enhanced activity with a local maximum in TC and hurricane frequency.

78 The origin of the discrepancy between the observed storm count and the model-simulated activity  
79 during the 2020 Atlantic hurricane season remains unclear and has not been comprehensively  
80 examined. Here we propose and evaluate a set of hypotheses to explain why the 2020 season,  
81 which was exceptionally active, was not captured by the ensemble spread of several state-of-the-art  
82 models. We group these hypotheses into two broad families and systematically test each using a  
83 combination of models, theoretical arguments, and observational and reanalysis datasets.

84 The first family of hypotheses considers whether deficiencies in models or observational datasets  
85 contributed to the poor simulation of 2020 Atlantic TC counts. Within this framework, we assess  
86 the following possibilities:  
87



78 FIG. 1. Annual frequency of (a) TCs, (b) hurricanes, and (c) major hurricanes from 1980–2024. The  
 79 observational record (black) is computed using the methodology and duration thresholds of Landsea et al. (2010)  
 80 to estimate the observed TC count in panel (a). Model simulations include AM2.5-C360 forced with observed and  
 81 bias-corrected SSTs from Chan et al. (2021) (blue) and HIRAM forced with the same SSTs (orange). Shading  
 82 denotes the full ensemble range (minimum–maximum) for each model (ten members for AM2.5-C360; five  
 83 members for HIRAM), and solid lines indicate ensemble means. Panel (c) shows only AM2.5-C360 results, as  
 84 HIRAM does not produce storms of sufficient intensity to be classified as major hurricanes.

- 94 1. Atmosphere-only models may exhibit structural limitations in their representation of TC  
95 formation, reducing their reliability in simulating interannual Atlantic TC variability.
- 96 2. Observed storm counts in recent decades, as shown in Fig. 1 (black lines), may be inaccurate.
- 97 3. Errors may be present in the observed monthly SST datasets used to force the models in 2020.
- 98 4. SST-forced models may not adequately represent the influence of observed aerosol changes on  
99 TC activity. Two major events in 2020 likely altered aerosol concentrations over the Atlantic  
100 basin. First, International Maritime Organization (IMO) regulations on the sulfur content of  
101 shipping fuel took effect on 1 January 2020, reducing maximum sulfur content from 3.5% to  
102 0.5%. Implemented to improve air quality, this policy reduced aerosol loading over the oceans  
103 and altered regional radiative fluxes (Diamond 2023; Jordan and Henry 2024; Zhang et al.  
104 2025b). Second, the onset of the COVID-19 pandemic led to substantial reductions in global  
105 emissions. Previous work suggests that decreased aerosol concentrations over North America  
106 and Europe can be associated with enhanced Atlantic TC activity (Murakami 2022, 2024).  
107 Because the SST-forced simulations analyzed here employ prescribed CMIP5 aerosol forcings  
108 rather than observed 2020 aerosol fields, the combined radiative and dynamical effects of these  
109 aerosol perturbations may not be represented.

110 The second family of hypotheses considers the possibility that the hyperactive 2020 season was  
111 a highly unlikely, but dynamically plausible, realization of the internal variability of the climate  
112 system. Under this interpretation, the large-scale environmental conditions in 2020 may have  
113 permitted a wide range of outcomes, including a low-probability hyperactive season. Subseasonal  
114 variability and internal atmospheric fluctuations could have amplified activity beyond the ensemble  
115 mean response, leading to an outcome that was not well captured by the models.

116 In the following sections we apply statistical analyses, dynamical diagnostics, DL-based climate  
117 simulations, and a theoretical framework to evaluate these competing explanations. The evidence  
118 presented in this paper supports the claim that the 2020 season was a low-probability outcome,  
119 rather than a structural failure in the models or observational record. At the same time, we cannot  
120 exclude the possibility that additional mechanisms not examined in this paper influenced the 2020  
121 Atlantic TC season.

## 122 **2. Methods and data**

### 123 *a. Dynamical Models*

124 To place the 2020 Atlantic TC season in the context of recent historical variability, we generate  
125 a multi-ensemble record of TC, hurricane, and major hurricane activity using two global TC-  
126 permitting atmospheric models developed at GFDL: AM2.5-C360 and HIRAM (Zhao et al. 2009).  
127 Following the methods of Levin et al. (2025), we conducted multi-ensemble historical experiments  
128 with both models. We generated ten (five) ensemble members for AM2.5-C360 (HIRAM), each  
129 forced with bias-corrected observed monthly SSTs from the HadISST dataset (Chan et al. 2021)  
130 over the period 1980–2024. From these simulations, we compute annual counts of TCs, hurricanes,  
131 and major hurricanes to construct a modeled range of historical Atlantic TC activity.

132 To evaluate hypothesis 4 from Section 1, which proposes that the 2020 reduction in atmospheric  
133 aerosols was not represented in the SST-forced simulations, we conduct additional experiments.  
134 We generate a five-member ensemble of AM2.5-C180 (a slightly lower-resolution configuration of  
135 AM2.5-C360 with approximately 50-km grid spacing) spanning 1980–2024. In these simulations,  
136 the model is forced with observed aerosol fields from the MERRA-2 reanalysis (Gelaro et al. 2017),  
137 rather than the CMIP5 aerosol reconstructions used in the historical integrations. This experiment  
138 isolates the effect of realistic interannual aerosol variability on modeled TC counts.

139 As a second approach, we perform an idealized modeling experiment to obtain additional samples  
140 and better quantify the relationship between sulfate and black carbon aerosols and Atlantic TC  
141 activity. Using the HIRAM model, we perform four simulations to isolate the effects of sulfate  
142 aerosols, which declined markedly in 2020 following the implementation of the IMO shipping  
143 regulation, and black carbon, which also decreased in 2020 due to reduced industrial activity and  
144 travel during the COVID-19 pandemic.

145 We perform a control experiment (cntl) in which the model is forced by the annual cycle of  
146 SSTs averaged over the period 1986–2005, following the methodology of Vecchi et al. (2019).  
147 This climatological SST cycle is repeated for 200 years following a 10-year spin-up, such that the  
148 200-year mean represents the model’s steady-state climatological baseline. We then perform three  
149 additional experiments using the same SST forcing as the control. In the first experiment, sulfate  
150 aerosols are removed over the North Atlantic (zeroSO4NA), and the model is integrated for 50

151 years. In the second experiment, sulfate aerosols are removed globally (zeroSO4global), and the  
152 model is again integrated for 50 years. In the final experiment black carbon emissions are removed  
153 globally (zeroBCglobal), and the model is integrated over 50 years. This serves as an exaggerated  
154 analogue to the global reduction in black carbon brought on by the COVID-19 pandemic.

155 To identify TCs and seed disturbances in both models, we follow the tracking procedure described  
156 in Levin et al. (2025). Hurricanes are defined as TCs that attain maximum winds exceeding  $33 \text{ m s}^{-1}$   
157 at least once during their lifetime. Major hurricanes are identified in AM2.5-C360 as storms whose  
158 maximum winds exceed  $45 \text{ m s}^{-1}$ , a threshold slightly lower than the observed  $50 \text{ m s}^{-1}$  standard  
159 because the model rarely produces storms at the observed major hurricane intensity. HIRAM  
160 does not reliably simulate storms of sufficient intensity to meet this major hurricane threshold, and  
161 therefore major hurricane statistics are reported only for AM2.5-C360.

## 162 *b. Statistical-Dynamical Model*

163 To characterize the range of plausible seasonal Atlantic TC counts over the recent historical  
164 period (1980–2024), we employ the statistical–dynamical model of Vecchi et al. (2011). This  
165 framework estimates the expected annual Atlantic TC count,  $\lambda$ , using a Poisson regression in  
166 which  $\lambda$  depends solely on SST.  $\lambda$  is modeled as a function of the mean seasonal SST anomaly  
167 in the Atlantic main development region (MDR) and the mean seasonal SST anomaly across the  
168 tropics, since these two predictors together have been shown to be a robust indicator of Atlantic TC  
169 activity in the present climate (Vecchi and Soden 2007; Villarini et al. 2011; Eusebi et al. 2025).  
170 Specifically, the logarithm of  $\lambda$  is modeled as the following linear function:

$$\lambda = \exp(1.707 + 1.388, SST_{MDR} - 1.521, SST_{TROP}), \quad (1)$$

171 where  $SST_{MDR}$  and  $SST_{TROP}$  are defined relative to the 1982–2005 climatology. The MDR is  
172 defined as  $10^{\circ}$ – $25^{\circ}$ N,  $80^{\circ}$ – $20^{\circ}$ W, and the tropical mean spans  $30^{\circ}$ S– $30^{\circ}$ N.

173 This formulation provides a full probabilistic distribution of seasonal outcomes conditional on  
174 the SST state. Thus, for each year in 1980–2024, the model yields a distribution of possible TC  
175 counts. We use this distribution to quantify the percentile rank of the observed 2020 season relative  
176 to SST-forced expectations.

177 We further use this model to evaluate hypothesis 3 from Section 1, which posits that discrepancies  
178 between observed and simulated 2020 TC counts may arise from inconsistencies in the observed  
179 SST datasets used to force atmosphere-only models. The AM2.5-C360 and HIRAM simulations  
180 analyzed here (Section a) are forced with a corrected version of the HadISST dataset (Chan et al.  
181 2021). To assess the sensitivity of the inferred TC distribution to the choice of SST product,  
182 we apply the statistical–dynamical model separately using three independent SST datasets: the  
183 Optimum Interpolation Sea Surface Temperature dataset (OISST; Huang et al. (2021)), the Hadley  
184 Centre Global Sea Ice and Sea Surface Temperature dataset (HadISST; Schneider et al. (2013)),  
185 and the Extended Reconstructed Sea Surface Temperature dataset (ERSST; Huang et al. (2017)).

186 Comparing the resulting modeled TC distributions across SST products serves two purposes.  
187 First, it enables us to evaluate the robustness of the estimated 2020 percentile to observational  
188 uncertainty in SST. Second, if substantial differences emerge across SST products, this would  
189 suggest that biases in the dataset used to force the atmosphere-only models could have contributed  
190 to their underestimation of 2020 activity. Conversely, consistency across SST products would  
191 indicate that SST dataset choice is unlikely to explain the model–observation discrepancy.

### 192 *c. DL-based Model*

193 Although the multi-ensemble historical integrations with AM2.5-C360 and HIRAM provide a  
194 dynamical range of Atlantic TC outcomes and require substantial computational resources, their  
195 ensemble sizes of ten and five members, respectively, are too small to fully characterize the  
196 probabilistic distribution of plausible 2020 seasonal outcomes.

197 Recent advances in deep-learning weather models have shown substantial promise for simulating  
198 TCs. Once trained, these models can be integrated efficiently with significantly lower computational  
199 costs compared to traditional dynamical models like AM2.5-C360 and HIRAM (e.g. (Bi et al.  
200 2023; Chen et al. 2023; Lam et al. 2023; Lang et al. 2024; Kochkov et al. 2024). In this study,  
201 we employ the Ai2 Climate Emulator version 2 (ACE2; Watt-Meyer et al. (2025)) to perform  
202 multi-ensemble annual simulations of historical Atlantic TC seasons, including 2020. We use a  
203 version of ACE2 trained on the ERA5 reanalysis (Hersbach et al. 2020). Previous studies have  
204 demonstrated that ACE2 is numerically stable over simulations spanning hundreds to thousands of  
205 years (Watt-Meyer et al. 2025) and can realistically reproduce TC characteristics across subseasonal

206 to interannual timescales (Chien et al. 2025). These properties make ACE2 a robust platform for  
207 generating large ensembles of Atlantic TC seasons and for investigating the range of plausible  
208 outcomes for extreme events such as the 2020 season.

209 We generate a 1,000-member SST-forced ensemble for each year during 2005–2020 (including  
210 the anomalously active 2005 and 2010 seasons) and for the anomalously inactive 1982 season.  
211 Following Chien et al. (2025), ensemble members for a given year are generated by repeatedly  
212 integrating the ACE2 model under identically fixed SST boundary forcing. For a given target year  
213 (e.g., 2020), observed SSTs from that year are prescribed and repeated cyclically. The model is  
214 then integrated autoregressively for 100 consecutive years under these repeating SST boundary  
215 conditions. Each simulated year represents one dynamically distinct realization of the same SST-  
216 forced year and is treated as an independent ensemble member.

217 To obtain 1,000 members efficiently, we perform ten parallel integrations (“chunks”), each  
218 producing 100 ensemble members via the 100-year repeated-SST integration described above.  
219 Distinct initial atmospheric states are used for each chunk. Specifically, we initialize ACE2  
220 from publicly available initial conditions and integrate the model forward for one year using SST  
221 boundary conditions from the year preceding the target year (e.g., 2019 SSTs when constructing the  
222 2020 ensemble). The final model state from this spin-up integration is then used to initialize one  
223 100-year repeated-SST chunk. This procedure is repeated to generate ten distinct initial conditions,  
224 yielding  $10 \times 100 = 1,000$  ensemble members. Because SST boundary conditions are held fixed  
225 within each ensemble while atmospheric initial conditions differ, the resulting spread reflects  
226 internal atmospheric variability under identical SST forcing. This design allows us to quantify the  
227 distribution of plausible seasonal TC outcomes conditioned on the observed SST state.

228 To detect TCs in ACE2, we follow the methodology of Chien et al. (2025) and Watt-Meyer et al.  
229 (2025), utilizing the TempestExtremes framework (Ullrich and Zarzycki 2017). By generating a  
230 1,000-member ensemble for the 2020 season, we can robustly estimate the percentile rank of the  
231 observed 2020 storm count within the modeled distribution and to characterize the tail behavior  
232 of seasonal variability. In doing so, we can assess whether the observed hyperactivity represents  
233 a statistically rare but dynamically plausible realization, consistent with the second family of  
234 hypotheses outlined in Section 1.

235 *d. Theoretical Framework*

236 To assess whether the large-scale environmental conditions in 2020 were favorable for a hyperac-  
 237 tive Atlantic season, and to evaluate whether the observed activity may represent a low-probability  
 238 but dynamically plausible outcome consistent with the second family of hypotheses outlined in  
 239 Section 1, we apply the theoretical framework of Hsieh et al. (2020) to ERA5 reanalysis data  
 240 (Hersbach et al. 2020) over the period 1980–2024.

241 The framework conceptualizes TC formation as a two-stage process involving precursor seed  
 242 disturbances and subsequent development into fully formed TCs. Under this formulation, the  
 243 annual number of North Atlantic TCs,  $N_{TC}$ , is approximated as

$$N_{TC} \approx SPI \times P(\Lambda), \quad (2)$$

244 where  $SPI$  is the seed propensity index, a proxy for the number of precursor seed disturbances,  
 245 and  $P(\Lambda)$  is a proxy for the nondimensional probability that a seed disturbance develops into a TC.  
 246 The seed propensity index is defined as

$$SPI = (-\omega) \cdot \frac{1}{1 + Z^{-1/\sigma}}, \quad (3)$$

247 where

$$Z = \frac{f + \zeta}{\sqrt{|\beta + \partial_y \zeta| U}}. \quad (4)$$

248 The variable  $\omega$  is the 500 hPa pressure coordinate vertical velocity ( $\omega < 0$  for upward motion),  
 249  $\sigma = 0.69$  is a nondimensional fitting parameter, and  $Z$  is nondimensional variable that represents  
 250 low level vorticity spinup.  $f$  is the Coriolis parameter,  $\beta$  is its meridional gradient,  $\zeta$  is 850 hPa  
 251 relative vorticity, and  $U$  is a constant wind speed of 20 m/s which is empirically fit in Hsieh et al.  
 252 (2020).

253 Next,  $P(\Lambda)$  is defined as

$$P(\Lambda) = \frac{1}{1 + (\Lambda_0/\Lambda)^{1/\gamma}}, \quad (5)$$

254 where

$$\Lambda = \frac{v_s \cdot \mathcal{X}}{PI}. \quad (6)$$

255 The variables  $\Lambda_0 = 0.014$  and  $\gamma = -0.9$  are dimensionless fitting parameters, and  $\Lambda$  denotes the  
256 ventilation index (Tang and Emanuel (2010); Tang and Emanuel (2012)).  $\nu_s$  is vertical wind  
257 shear between 250 hPa and 850 hPa, PI is potential intensity, and  $\chi$  is a dimensionless variable  
258 representing entropy deficit.

259 In this study, we extend the existing framework to investigate both seasonal and subseasonal  
260 variability by incorporating monthly mean and daily environmental data from ERA5, averaged  
261 over the tropical Atlantic ( $10^\circ$ – $30^\circ$  N) during June through November, to derive a proxy for TC  
262 activity. Basin-wide means are calculated over a region extending beyond the Main Development  
263 Region ( $10^\circ$ – $25^\circ$  N,  $80^\circ$ – $20^\circ$  W) to include the Gulf of Mexico, in order to account for the high  
264 concentration of storms that occurred there in 2020 (Fig. S4). Including the Gulf of Mexico ensures  
265 that differences in TC track locations among years are appropriately represented in the analysis.  
266 To our knowledge, this TC proxy ( $N_{TC} \approx SPI \times P(\Lambda)$ ) has not been computed on subseasonal  
267 timescales to study subseasonal TC variability.

268 We also construct an alternative proxy for annual Atlantic TC counts that explicitly incorporates  
269 tracked precursor seeds. In this formulation, annual TC activity is approximated as

$$N_{TC} \approx N_s \times P(\Lambda), \quad (7)$$

270 where  $N_s$  denotes the observed annual count of explicitly tracked TC seeds. Here, seed frequency  
271 is diagnosed directly from reanalysis data, allowing us to more explicitly separate variability in  
272 seed frequency from variability in development probability.

### 273 **3. Results**

#### 274 *a. Testing the first hypothesis family*

275 In this section, we present the results to evaluate the first family of hypotheses as to why  
276 the models poorly represented the hyperactive 2020 Atlantic TC season: whether there were  
277 fundamental deficiencies in the models or observational datasets.

278 1) HYPOTHESIS NUMBER ONE

279 This hypothesis poses that the dynamical atmosphere-only models used in this study to generate  
280 the historical TC record in Figure 1 (AM2.5-C360 and HIRAM) may be limited in their ability to  
281 represent TC genesis, and thus, are unreliable to assess Atlantic TC interannual variability.

282 This explanation appears unlikely. In addition to the demonstrated skill of AM2.5-C360 and  
283 HIRAM in reproducing the long-term historical variability of Atlantic TC activity (Levin et al.  
284 2025), the influence of SSTs on TC frequency and intensity (Chan et al. 2021), and the annual TC  
285 cycle (Yang et al. 2021), it is notable that the anomalous 2020 season also lies at or beyond the  
286 ensemble range in other independent modeling systems. Seasonal forecasts from physics-based  
287 coupled models such as GFDL SPEAR and FLOR (Murakami et al. 2025), as well as from DL-  
288 based models such as NeuralGCM (Zhang et al. 2025a), similarly place 2020 at the edge or outside  
289 their ensemble distributions. The fact that multiple structurally distinct modeling frameworks  
290 fail to encompass the observed 2020 hyperactivity within their ensemble spread suggests that a  
291 model-specific deficiency is unlikely to be the sole explanation.

292 2) HYPOTHESIS NUMBER TWO

293 This hypothesis posits that the observed storm counts in recent decades, shown in Fig. 1, may  
294 be inaccurate. Although it is not possible to retrospectively reanalyze past seasons to verify the  
295 historical record, confidence in TC observations during the modern era is high. Since the 1960s,  
296 operational monitoring has relied on polar-orbiting and geostationary satellites, supplemented  
297 beginning in the 1980s by routine aircraft reconnaissance. In more recent decades, scatterometers  
298 and microwave radiometers have further improved the detection and characterization of TCs (see  
299 Supplemental Fig. SB1 of Klotzbach et al. (2022)).

300 Our analysis focuses on the post-1980 period shown in Fig. 1, when these modern observing  
301 systems were consistently in place. The launch of advanced geostationary satellites, including  
302 GOES-16 and GOES-17 beginning in 2016, further enhanced spatial and temporal resolution, in-  
303 creasing confidence in estimates of recent storms, including those in 2020. Although observational  
304 uncertainty is larger prior to the satellite era and may be somewhat higher before 2016 relative to  
305 the most recent years, the modern record is widely regarded as reliable for basin-wide TC counts.

306 Moreover, Figs. 1b and c show that the 2020 season was also anomalously active in terms of  
307 hurricanes and major hurricanes. These more intense systems are less susceptible to detection  
308 ambiguity than TCs, since high wind speeds, organized structure, and satellite signatures are more  
309 clearly identifiable. Given the robustness of the modern observing network and the particularly clear  
310 identification of intense storms, it is unlikely that errors in the observed 2020 record can explain  
311 the discrepancy between the observed activity and the ensemble range of the model simulations.

### 312 3) HYPOTHESIS NUMBER THREE

313 The third hypothesis proposes that the discrepancy between the observed 2020 TC count and  
314 simulated ensemble spread arises from errors in the SST dataset forcing the atmosphere-only  
315 models. To evaluate this possibility, we apply the statistical–dynamical model of Vecchi et al.  
316 (2011), which uses SST as the predictor of Atlantic TC activity. Generate seasonal TC distributions  
317 for 1980–2024 using three independent SST products as input: OISST, HadISST, and ERSST.

318 The resulting SST-based seasonal TC activity statistical reconstructions are shown in Fig. S1.  
319 Across the historical period, the model captures a substantial fraction of the observed interannual  
320 variability, with correlations between modeled and observed TC counts ranging from  $r = 0.66$  to  
321  $r = 0.70$  across the three SST products. Historically active seasons such as 1995, 2005, and 2010,  
322 as well as relatively inactive seasons such as 1982 and 2009, fall within the 90% confidence interval  
323 of the modeled distribution.

324 For the 2020 season, two key findings emerge. First, although the three SST datasets exhibit  
325 differences in global mean trends and regional structure (Menemenlis et al. 2025), their predictions  
326 for 2020 are nearly identical when used in the statistical–dynamical TC model. The mean predicted  
327 TC count ranges from 10.9 to 11.8 storms across the three products, demonstrating close agreement.  
328 Based on this consistency, we have no evidence to support the presence of a fundamental error in  
329 the HadISST dataset, which was used to force the dynamical simulations. Second, all three SST  
330 products indicate that 2020 should have been only moderately active. In each case, the observed  
331 TC count lies well above the 90% confidence bound of the modeled distribution. Thus, even when  
332 accounting for uncertainty across independent SST datasets, seasonal mean SST conditions do not  
333 support an expectation of hyperactive activity comparable to what was observed.

#### 334 4) HYPOTHESIS NUMBER FOUR

335 Our fourth hypothesis posits that the failure of the observed 2020 TC count to fall within the  
336 ensemble range of the AM2.5-C360 and HIRAM simulations may reflect limitations of SST-forced  
337 models in capturing the impacts of the abrupt aerosol perturbations. If these changes altered  
338 the large-scale environment in a manner favorable to TC development, but were not adequately  
339 represented in the model forcing, they could have contributed to the model–observation discrepancy.

340 To evaluate this hypothesis, we employ two complementary approaches. First, we perform a five-  
341 member AM2.5-C360 ensemble integration over 1980–2024 using observed aerosol concentrations  
342 derived from reanalysis, in contrast to the historical simulations shown in Fig. 1, which use  
343 prescribed CMIP5 aerosol forcing. Second, we conduct idealized sensitivity experiments in which  
344 sulfate and black carbon aerosols are substantially reduced to emulate an exaggerated analogue of  
345 the 2020 aerosol decline. The experimental design is described in Section 2.

346 For the first approach, the resulting Atlantic TC counts are shown in Fig. S2 alongside the  
347 observed record. The multi-member simulation reproduces interannual variability reasonably  
348 well, with a correlation of  $r = 0.61$  relative to observations. However, even when forced with  
349 observed aerosol concentrations, the model simulates 2020 as a relatively inactive season. The  
350 absence of a change in simulated Atlantic TC activity when including observed aerosols suggests  
351 that any radiative or dynamical effects associated with the 2020 aerosol reduction were either small  
352 or already reflected indirectly in the observed SST boundary conditions. This result indicates that  
353 aerosol forcing alone does not reconcile the simulated and observed TC counts for 2020.

354 The idealized experiments yield a similar conclusion. The distributions of annual Atlantic TC  
355 counts from the control and aerosol-reduction simulations are shown in Fig. S3. The distributions  
356 are broadly similar, with all three experiments yielding an average of approximately twelve Atlantic  
357 TCs per year. A Kolmogorov–Smirnov test comparing each experimental simulation to the control  
358 indicates that we cannot reject the null hypothesis that the annual TC counts from the zeroSO4NA  
359 and cntl simulations are drawn from the same distribution ( $p = 0.74$ ). Similarly, we cannot  
360 reject the null hypothesis that the zeroSO4global and cntl simulations originate from the same  
361 distribution ( $p = 0.28$ ), nor can we reject the null hypothesis that the zeroBCglobal and cntl  
362 simulations originate from the same distribution ( $p = 0.99$ ). These results suggest that, within this  
363 modeling framework, the direct radiative effects of prescribed low-frequency (>monthly) aerosol

364 variations on atmospheric heating do not exert a statistically robust influence on Atlantic TC activity.  
365 This conclusion does not preclude potential aerosol influences operating through SST-mediated  
366 pathways or synoptic-scale interactions, which are not explicitly represented in these experiments.

367 *b. Testing the second hypothesis family*

368 In this section, we evaluate the second hypothesis family, which considers the possibility that the  
369 hyperactive 2020 season was a highly unlikely but dynamically plausible outcome.

370 1) STATISTICAL ANALYSIS OF MODELED TC ACTIVITY

371 To evaluate this hypothesis, we first examine the historical ensembles from the dynamical AM2.5-  
372 C360 and HIRAM models shown in Fig. 1. Rather than treating 2020 in isolation, we quantify  
373 how often the observed storm count falls outside the modeled ensemble spread across the entire  
374 45-year record.

375 Assuming the dynamical models are well calibrated, the observed record can be interpreted as  
376 an additional equally likely realization drawn from the same distribution as the model ensemble  
377 members. Under this assumption, the AM2.5-C360 system effectively contains 11 realizations  
378 per year, comprising 10 model members plus the observational record, while HIRAM contains  
379 6 realizations per year, comprising 5 model members plus the observational record. To see the  
380 implication of this assumption, consider a simple analogy. Suppose we place 1 red ball (the  
381 observation) and  $n - 1$  blue balls (the ensemble members) in a line at random. Because all  
382 permutations are equally likely, the red ball is equally likely to occupy any of the  $n$  positions. The  
383 red ball lies at one of the two ends with probability  $2/n$ . In our application, the “ends” correspond  
384 to the smallest or largest value among the  $n$  realizations. Thus, if the system is well calibrated, the  
385 probability that the observation lies outside the ensemble range in any given year (i.e., is either the  
386 minimum or maximum among the  $n$  realizations) is

$$P(\text{outside ensemble range}) = \frac{2}{n}.$$

387 For AM2.5-C360,  $n = 11$ , giving the probability that the observation lies outside the ensemble  
388 range for in a given year as

$$\frac{2}{11} \approx 0.18.$$

389 For HIRAM,  $n = 6$ , giving the probability that the observation lies outside the ensemble range for  
390 in a given year as

$$\frac{2}{6} = \frac{1}{3}.$$

391 The expected values, or expected number of instances when the observational record lies outside  
392 the ensemble range during the historical period, are therefore

$$\mathbb{E}[X] = 45 \times \frac{2}{11} \approx 8$$

393 for AM2.5-C360 and

$$\mathbb{E}[X] = 45 \times \frac{1}{3} = 15$$

394 for HIRAM.

395 In Fig. 1, the observed record lies outside the AM2.5-C360 ensemble spread 6 times for total  
396 TCs, 3 times for hurricanes, and 5 times for major hurricanes. These outcomes are well within  
397 sampling variability and are therefore consistent with a calibrated system. Similarly, for HIRAM,  
398 the observed record lies outside the ensemble spread 15 times for TCs and 12 times for hurricanes,  
399 both close or equal to the expectation of 15 exceedances.

400 Thus, even in a perfectly calibrated system with only five to ten ensemble members, it is expected  
401 that the observation will fall outside the ensemble range multiple times over a 45-year period.  
402 Although 2020 stands out visually because it lies outside the ensemble spread simultaneously for  
403 TCs, hurricanes, and major hurricanes, similar exceedances occur elsewhere in the historical record  
404 (e.g., 2013 and 1996).

405 At the same time, the limited ensemble sizes of AM2.5-C360 and HIRAM (10 and 5 members,  
406 respectively) constrain our ability to precisely estimate tail probabilities. For this reason, while the  
407 dynamical ensembles suggest that occasional out-of-range seasons are expected, they do not allow  
408 a precise quantification of how unlikely a hyperactive season such as 2020 may have been. This  
409 limitation motivates the use of the ACE2 DL-based model to generate a much larger ensemble of  
410 seasonal TC counts and more robustly characterize the distribution's tail behavior.

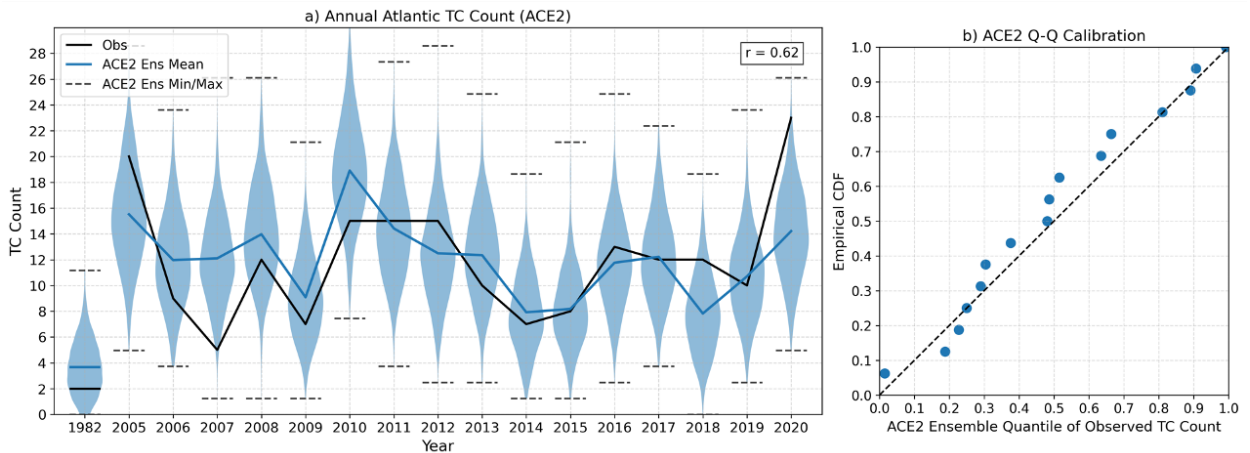
411 To determine the probability of a hyperactive 2020 Atlantic TC season under the observed 2020  
412 SST forcing, we generate a 1,000-member ensemble for that year, each representing a plausible  
413 realization of the season (Section c). We also generate a 1,000-member ensemble for each year

414 within the 1982 and 2005-2020 period, spanning both active and inactive seasons that are captured  
415 within the ensemble spread of dynamical models, including 1982, 2005, 2009, and 2010 (Fig. 1).  
416 Our comparison across years in the recent record allows us to assess whether the behavior of the  
417 DL-based model diverges substantially from that of physics-based atmosphere-only models. This  
418 large-ensemble technique also enables us to capture the full spectrum of possible 2020 TC season  
419 outcomes under the observed SST forcing.

420 The observed annual TC counts and the distribution of simulated TC counts from the 1,000-  
421 member historical ACE2 ensemble are shown in Figure 2a. ACE2 exhibits a moderate positive  
422 correlation between the observed TC counts and the ensemble-mean simulated counts ( $r = 0.62$ ),  
423 indicating skill in distinguishing between relatively active and inactive seasons due to SST and  
424 carbon dioxide external forcing alone. The ensemble mean peaks during active seasons such as  
425 2005 and 2010, and shows local minima during inactive seasons such as 2009 and 2014, consistent  
426 with the observed variability.

438 Beyond reproducing the observed mean-state variability, the ensemble exhibits substantial inter-  
439 annual spread. For each of the 17 seasons shown, the simulated range of TC counts (the difference  
440 between the ensemble minimum and maximum) spans roughly 10 to 26 storms. For instance,  
441 in 2005 the ensemble indicates that between approximately five and 28 TCs were dynamically  
442 plausible, whereas in the relatively inactive 2014 season the simulated range extends from one to  
443 19 TCs. Despite this considerable variability, the observed TC count falls within the ensemble  
444 distribution for most seasons in the historical record. Furthermore, the calibration Q-Q plot (Fig.  
445 2b) shows the empirical cumulative distribution function closely tracking the 1:1 line, indicating  
446 that the ACE2 ensemble spread is well calibrated. In other words, the verifying observational quan-  
447 tile is approximately uniformly distributed across years, suggesting that the ensemble dispersion  
448 realistically represents seasonal uncertainty.

449 Although ACE2 generally distinguishes between active and inactive years, visual inspection  
450 of Figure 2a indicates that discrepancies between the ensemble mean and observations are the  
451 largest prior to 2010 and in 2020, while agreement improves during the 2010–2019 period. This is  
452 consistent with the fact that these latter years overlap with the model’s training period of 2011-2019  
453 (Watt-Meyer et al. 2025).



427 FIG. 2. (a) Annual Atlantic tropical cyclone (TC) counts for 1982 and 2005–2020. The adjusted observational  
 428 record computed using the methods from Landsea et al. (2010) is shown in black. Blue violin plots depict the  
 429 distribution of simulated TC counts from the 1,000-member ACE2 ensemble forced with observed SSTs, with  
 430 the ensemble mean indicated by the solid blue line, and ensemble minimum and maximum indicated by the  
 431 dashed dark gray lines. The correlation between the ensemble-mean TC frequency and the observed counts  
 432 is shown in the upper-right corner. (b) Quantile–quantile (Q–Q) calibration diagnostic of ACE2 over the 17  
 433 verification years. For each year, we compute the percentile (quantile) at which the observed TC count falls  
 434 within the 1,000-member ensemble distribution. This yields one quantile value per year (17 total). We then plot  
 435 the empirical cumulative distribution function (CDF) of these 17 quantiles. If the ensemble is well calibrated,  
 436 these verification quantiles should be uniformly distributed across years, and the empirical CDF should align  
 437 with the 1:1 line (black dashed).

454 There are several years in which the observed TC count falls near the extreme tails of the ACE2  
 455 ensemble distribution. One such case is 2007, an anomalously inactive season with only five  
 456 observed TCs. The 1,000-member ACE2 ensemble, forced with observed 2007 SSTs, simulated a  
 457 plausible range of approximately one to 26 storms, with an ensemble mean of 12. Only 15 of the  
 458 1,000 members produced five or fewer TCs, indicating that the realized season corresponds to a  
 459 1.5% lower-tail event within the modeled distribution. An even more pronounced tail event occurs  
 460 in 2020. The ensemble simulates a mean of approximately 14 TCs (Table 1), compared to the  
 461 23 storms observed. Only 37 ensemble members produce at least 20 storms (3.7%), and just five  
 462 members simulate 23 or more storms (0.5%). Thus, under the observed 2020 SST forcing, ACE2

469 TABLE 1. Modeled distribution of 2020 seasonal TC counts using a statistical-dynamical model with three  
 470 SST products as inputs and the DL-based ACE2 1,000-member ensemble model. For each modelled TC count  
 471 distribution we show the distribution’s mean, quantile at which the observed 23 TC counts in 2020 verified  
 472 against the modeled distribution, and the corresponding percent of such an event.

Model	Model Mean TC count	Verified Quantile	Event Percent
Statistical-Dynamical (HadISST)	11.0	0.999	0.1%
Statistical-Dynamical (ERSST)	11.8	0.997	0.3%
Statistical-Dynamical (OISST)	10.9	0.999	0.1%
ACE2 1,000 member ensemble	14.1	0.995	0.5%

463 characterizes the realized season as a rare but physically plausible outcome, verifying at the 99.5th  
 464 percentile of the modeled distribution.

465 To place this result in broader context, Table 1 compares ACE2 with the statistical–dynamical  
 466 Poisson model described in Eq. 1, forced separately with three SST datasets (HadISST, ERSST, and  
 467 OISST). All models consistently indicate that the boundary conditions in 2020 were not expected  
 468 to produce such an exceptional season, with event probabilities ranging from 0.1% to 0.5%.

473 Although a 0.5% event is highly unlikely in any single year, its occurrence over a multidecadal  
 474 record is less implausible. Assuming independence between seasons, the probability of observing  
 475 at least one 0.5% event over a 45-year period (e.g., 1980–2024) is

$$P(\text{At least one } 0.5\% \text{ event}) = 1 - (0.995)^{45} \approx 0.20. \quad (8)$$

476 Thus, an event with a 0.5% annual probability has roughly a 20% chance of occurring at least once  
 477 in a 45-year historical record.

478 To evaluate how ensemble size influences the ability to capture the full range of plausible 2020  
 479 Atlantic TC outcomes, and to demonstrate how reliance on the ensemble mean alone can obscure  
 480 tail risk, we conduct a resampling experiment using the 1,000-member ACE2 simulation of the  
 481 2020 season. From this large ensemble, we randomly draw either 10 or 15 members without  
 482 replacement and repeat this procedure 10,000 times. These sample sizes mimic the ensemble sizes  
 483 typically used in physics-based seasonal forecasting systems, which often consist of only 10–15  
 484 members (e.g., Murakami et al. (2025)).

491 TABLE 2. The percentage of 10,000 resampled realizations of annual Atlantic TC counts from the ACE2 model  
 492 that satisfy specific activity thresholds. Each realization is constructed by randomly selecting either 10 or 15  
 493 ensemble members from the 1,000 ACE2 simulations of the 2020 season, without replacement, and repeating  
 494 this sampling process 10,000 times.

Criteria across all samples (%)	10 ensembles	15 ensembles
$\geq 1$ ens with at least 20 TCs	32.99%	44.96%
$\geq 2$ ens with at least 20 TCs	5.86%	12.06%
$\geq 1$ ens with at least 23 TCs	8.03%	11.51%
$\geq 2$ ens with at least 23 TCs	0.24%	0.56%
mean $> 12$ TCs ('active season')	97.96%	99.62%
mean $< 12$ TCs ('inactive season')	2.04%	0.38%
mean $> 17$ TCs (' $+1\sigma$ season')	0.65%	0.16%
mean $< 7$ TCs (' $-1\sigma$ season')	0.00%	0.00%

485 For each resampled ensemble, we evaluate whether specific activity thresholds are met (Table  
 486 2). In particular, we assess the probability that at least one or at least two members simulate (i)  
 487 a season with  $\geq 20$  TCs (comparable to other hyperactive years such as 2005) and (ii) a season  
 488 with  $\geq 23$  TCs, matching the observed 2020 count. We also classify seasons using the ensemble  
 489 mean. An “active” season is defined as one with a mean  $\geq 12$  TCs, consistent with the 2005–2020  
 490 observed mean (approximately 12 storms).

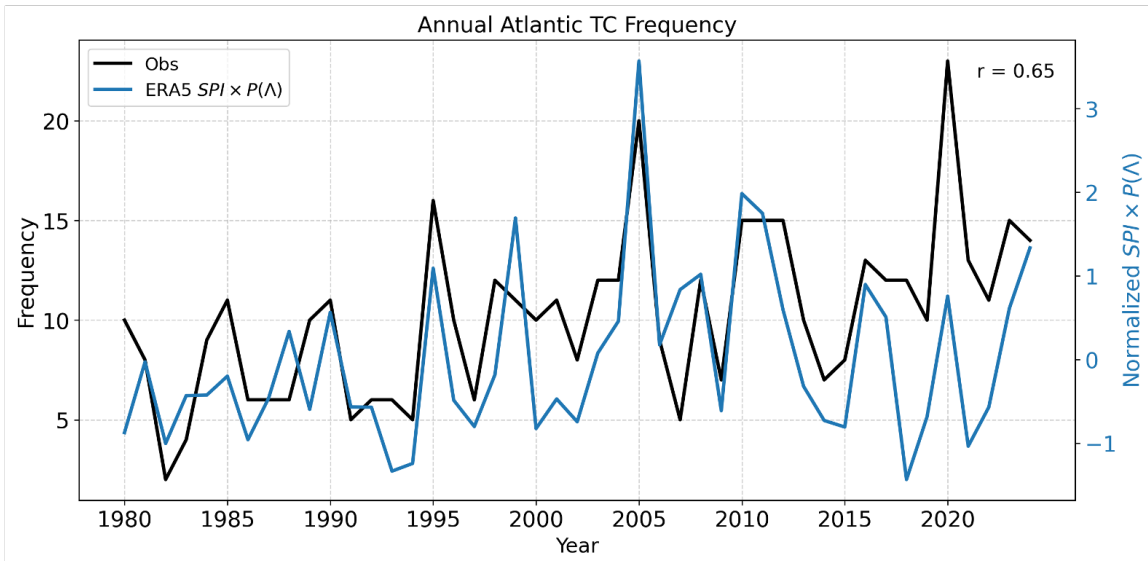
495 A 10-member (15-member) ensemble includes at least one member with  $\geq 23$  TCs in approx-  
 496 imately 8% (12%) of realizations, suggesting that even with a limited ensemble, there is a non-  
 497 negligible chance that a hyperactive scenario would appear within the ensemble spread. At the  
 498 same time, reliance on the ensemble mean would have masked much of this tail behavior. Nearly  
 499 all resampled ensembles (98–100%) produce a mean above 12 storms, correctly indicating that  
 500 2020 was likely to be active. However, extremely active outcomes are rarely reflected in the mean:  
 501 fewer than 1% of samples exceed the  $+1\sigma$  threshold ( $\geq 17$  storms), and none fall below  $-1\sigma$ .

## 502 2) LARGE-SCALE ENVIRONMENTAL CONDITIONS IN 2020

503 To further evaluate the second family of hypotheses, that the hyperactive 2020 season was a highly  
 504 unlikely but dynamically plausible realization of the climate system, we examine the large-scale  
 505 environmental conditions that prevailed during that year. Internal atmospheric variability operating

506 on subseasonal timescales could have amplified activity beyond what would be anticipated from  
 507 seasonal-mean conditions alone.

508 To test this idea, we leverage ERA5 reanalysis data in combination with the theoretical TC proxy  
 509 introduced by Hsieh et al. (2020), defined as  $N_{TC} \approx SPI \times P(\Lambda)$ , which approximates seasonal  
 510 TC counts as a function of the large-scale environment. We compute the seasonally and tropical  
 511 Atlantic basin-averaged TC proxy using monthly mean ERA5 inputs for the period 1980–2024  
 512 ( $SPI \times P(\Lambda)$ , Fig. 3). This framework reproduces a substantial portion of the observed interannual  
 513 variability in Atlantic TC activity, yielding a correlation of  $r = 0.65$  between observed and both  
 514 proxy-derived TC counts. Thus, seasonal-mean large-scale environmental conditions explain much  
 515 of the historical variability in Atlantic TC activity.



516 FIG. 3. Observed annual Atlantic tropical cyclone (TC) counts (black; left y-axis), approximated annual TC  
 517 frequency ( $SPI \times P(\Lambda)$ ); blue; right y-axis) derived from seasonally and TC main development region (MDR)-  
 518 averaged monthly ERA5 data for 1980–2024. The parameterized TC frequencies are standardized using Z-score  
 519 normalization, defined as  $Z(x) = (x - \mu_x) / \sigma_x$ , where  $x$  is the data point,  $\mu_x$  is the mean over the full record,  
 520 and  $\sigma_x$  is the standard deviation. The correlation coefficient between observed and approximated TC counts is  
 521 shown in the upper-right corner of the panel.

522 However, a clear discrepancy emerges in 2020, when the observed TC count substantially exceeds  
 523 the proxy estimate (blue line in Fig. 3). When the 2020 season is excluded, the correlation between

524 the observed counts and the seasonal  $\text{SPI} \times P(\Lambda)$  (blue line) increases to  $r = 0.70$ . Deviations  
525 between the proxy and observations are also evident in the surrounding years, particularly from  
526 2018 to 2021. These results indicate that, based on seasonally averaged large-scale conditions  
527 alone, 2020 did not appear exceptionally favorable for hyperactivity.

528 To determine whether subseasonal atmospheric variability contributed to the inability of the  
529 HIRAM and AM2.5-C360 models to capture a hyperactive 2020 TC season within their ensemble  
530 range, we further analyze the TC proxy in ERA5 data on daily and subseasonal timescales. In  
531 addition to computing the TC proxy using exclusively monthly input data, we also compute the  
532 proxy using daily data. For the 2020, 2010, and 2005 seasons, we calculate the monthly product  
533 of  $\text{SPI} \times P(\Lambda)$  (our TC proxy) using four distinct approaches:

- 534 1.  **$\text{SPI}_{\text{Daily}} \times P(\Lambda)_{\text{Daily}}$** : Daily input data are used to compute both SPI and  $P(\Lambda)$ . Monthly  
535 means of these daily values are then computed, multiplied, and averaged over the tropical  
536 Atlantic ( $10^\circ\text{--}30^\circ\text{ N}$ ).
- 537 2.  **$\text{SPI}_{\text{Monthly}} \times P(\Lambda)_{\text{Monthly}}$** : Monthly mean input data are used to compute SPI and  $P(\Lambda)$ . These  
538 fields are then multiplied and averaged over the tropical Atlantic ( $10^\circ\text{--}30^\circ\text{ N}$ ).
- 539 3.  **$\text{SPI}_{\text{Daily}} \times P(\Lambda)_{\text{Monthly}}$** : Daily input data are used to compute SPI, which is then averaged to  
540 monthly means. These values are multiplied by  $P(\Lambda)$  computed from monthly mean input  
541 data and averaged over the tropical Atlantic ( $10^\circ\text{--}30^\circ\text{ N}$ ).
- 542 4.  **$\text{SPI}_{\text{Monthly}} \times P(\Lambda)_{\text{Daily}}$** : Monthly input data are used to compute monthly SPI. Daily input  
543 data are used to compute daily  $P(\Lambda)$ , which is then averaged to monthly means. These values  
544 are multiplied and averaged over the tropical Atlantic ( $10^\circ\text{--}30^\circ\text{ N}$ ).

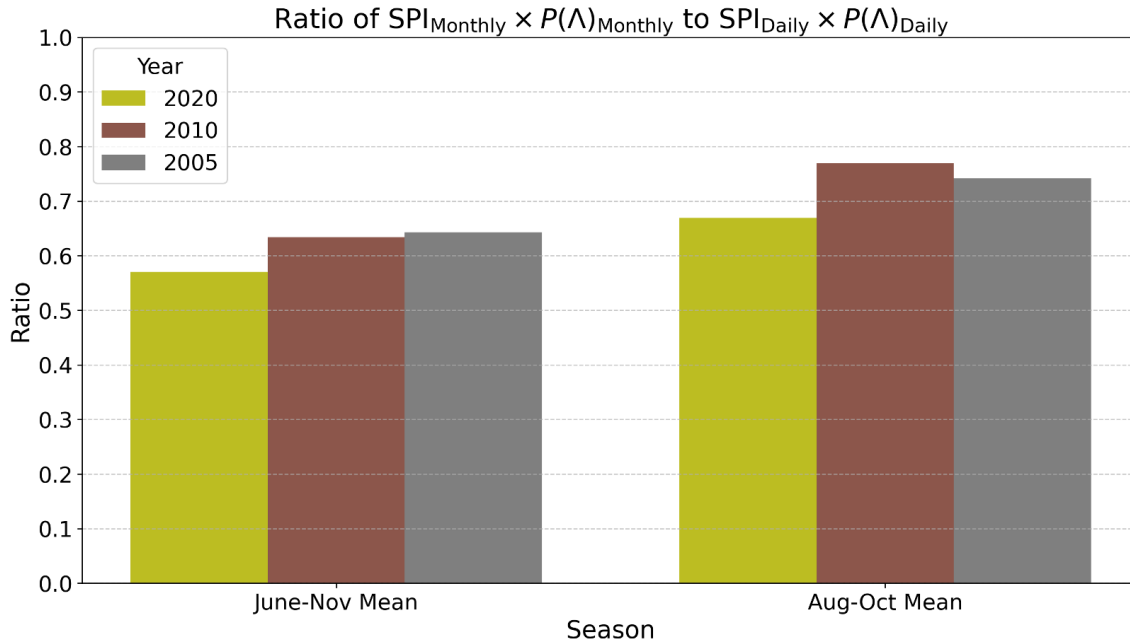
545 The distinction among the four approaches lies in the order of operations: whether monthly means  
546 are taken prior to computing SPI and  $P(\Lambda)$ , or whether these quantities are first computed daily and  
547 then averaged to monthly scales. This framework enables us to assess the influence of subseasonal  
548 atmospheric variability on the TC proxy. When approaches (1) and (2) closely agree for a given  
549 season, it suggests that subseasonal atmospheric variability plays a limited role, indicating higher  
550 seasonal TC predictability from monthly mean boundary conditions. We calculate the seasonally  
551 averaged ratio of approaches (1) and (2) for the 2005, 2010, and 2020 seasons. We select the 2010

552 and 2005 seasons because, despite their high activity, both were anticipated to be active by the the  
553 ensemble spread of the HIRAM and AM2.5-C360 models forced with monthly SSTs (Fig. 1).

554 The seasonally-averaged ratios are shown in Fig. 4. For both the full TC season (June–November)  
555 and the peak period (August–October), the 2020 season exhibits the greatest deviation from one,  
556 with the lowest values (0.57 and 0.67), indicating the largest disagreement between approaches  
557 (1) and (2) and weakest seasonal TC predictability from monthly mean boundary conditions. In  
558 contrast, the ratios for 2010 (0.63 and 0.77) and 2005 (0.64 and 0.74) are closer to one, suggesting  
559 higher predictability for seasonal TC activity from monthly mean conditions. These results are  
560 consistent with the consensus across the ensemble spread of both DL and dynamical models that the  
561 2005 and 2010 seasons would be active. These results also suggest that monthly conditions alone  
562 were insufficient to represent the conditions leading to the exceptional activity of 2020. While this  
563 framework helps diagnose differences in seasonal TC predictability with monthly mean boundary  
564 conditions, it does not fully explain the physical drivers behind the extreme activity of 2020.

570 The monthly and daily TC-proxy calculations for 2005, 2010, and 2020 (Fig. 5) provide further  
571 insight into the role of subseasonal variability in seasonal outcomes. To isolate which proxy  
572 component (either the seed component (SPI) or the transition component ( $P(\Lambda)$ )) contributes most  
573 strongly to subseasonal sensitivity, we compare two hybrid formulations:  $SPI_{\text{Daily}} \times P(\Lambda)_{\text{Monthly}}$   
574 and  $SPI_{\text{Monthly}} \times P(\Lambda)_{\text{Daily}}$ . Across all three active seasons, the orange (monthly-only) and red  
575 (monthly SPI, daily  $P(\Lambda)$ ) curves remain relatively close, whereas the gray curve (daily SPI,  
576 monthly  $P(\Lambda)$ ) departs more substantially. This behavior indicates that subseasonal variability in  
577 the seed component (SPI), contributes more strongly to subseasonal variability than subseasonal  
578 fluctuations in the environmental transition probability  $P(\Lambda)$ .

587 Therefore, we test whether seed disturbances contributed to the hyperactive 2020 TC season  
588 emerging as a rare realization within the ensemble spread of multiple models. To do so, we  
589 examine explicitly tracked Atlantic TC seeds from three independent ERA5-based datasets (Moon  
590 et al. (2025); Vishnu et al. (2020); Ikehata and Satoh (2021)), in addition to our own tracking  
591 methodology. Each method tracks storms using 6-hourly June–November North Atlantic ERA5  
592 data. The resulting seed counts are shown in Fig. 6. These differing approaches yield different  
593 mean seed climatologies, yet they share broad interannual patterns. Notably, none identifies 2020

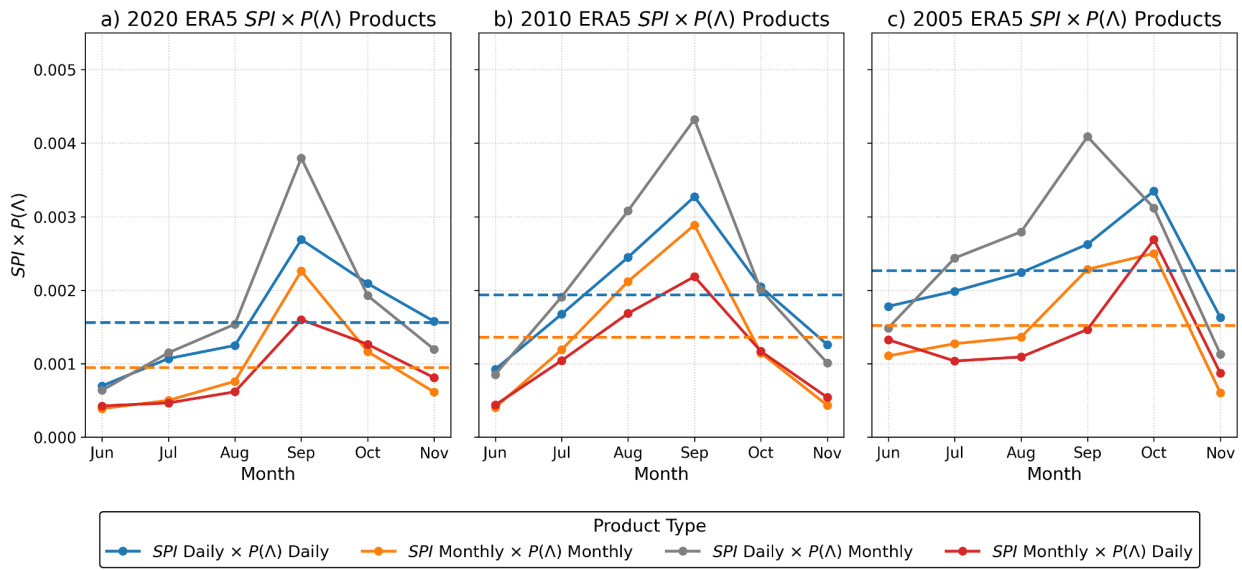


565 FIG. 4. The seasonally averaged ratio  $SPI_{\text{Monthly}} \times P(\Lambda)_{\text{Monthly}}$  (approach 2) to  $SPI_{\text{Daily}} \times P(\Lambda)_{\text{Daily}}$  (approach  
 566 1) is shown for the full TC season of June–November and the most active portion of the season, August–November  
 567 for 2020 (olive bars), 2010 (brown bars), and 2005 (gray bars). A higher ratio closer to one implies greater  
 568 predictability. We observe the ratio to be lower in 2020 than 2010 and 2005 for the full season and most active  
 569 portion of the season.

594 as a local maximum in seed count (Fig. 6). If the hyperactivity of 2020 were driven by anomalously  
 595 many seeds, we would expect at least one tracking methodology to identify an extreme seed year.

605 We then incorporate explicitly tracked seeds into the TC proxy, replacing SPI with observed  
 606 seed count to compute  $N_{TC} \approx \text{Seeds} \times P(\Lambda)$ , where  $P(\Lambda)$  is derived from seasonal monthly ERA5  
 607 conditions. This modified proxy reproduces a substantial portion of observed interannual variability  
 608 (correlations  $r = 0.63\text{--}0.69$ ) and successfully captures both inactive and active years such as 2005  
 609 and 2010. Yet across all three seed-tracking methodologies, the proxy converges on a moderately  
 610 active 2020 season of roughly twelve storms, below the observed 23.

611 Thus, even when incorporating subseasonally tracked seeds and accounting for observed atmo-  
 612 spheric variability within the proxy framework, the 2020 atmospheric conditions do not appear  
 613 conducive to a hyperactive TC season. While subseasonal variability appears more influential in  
 614 2020 than in other active seasons, suggesting reduced predictability from monthly mean boundary

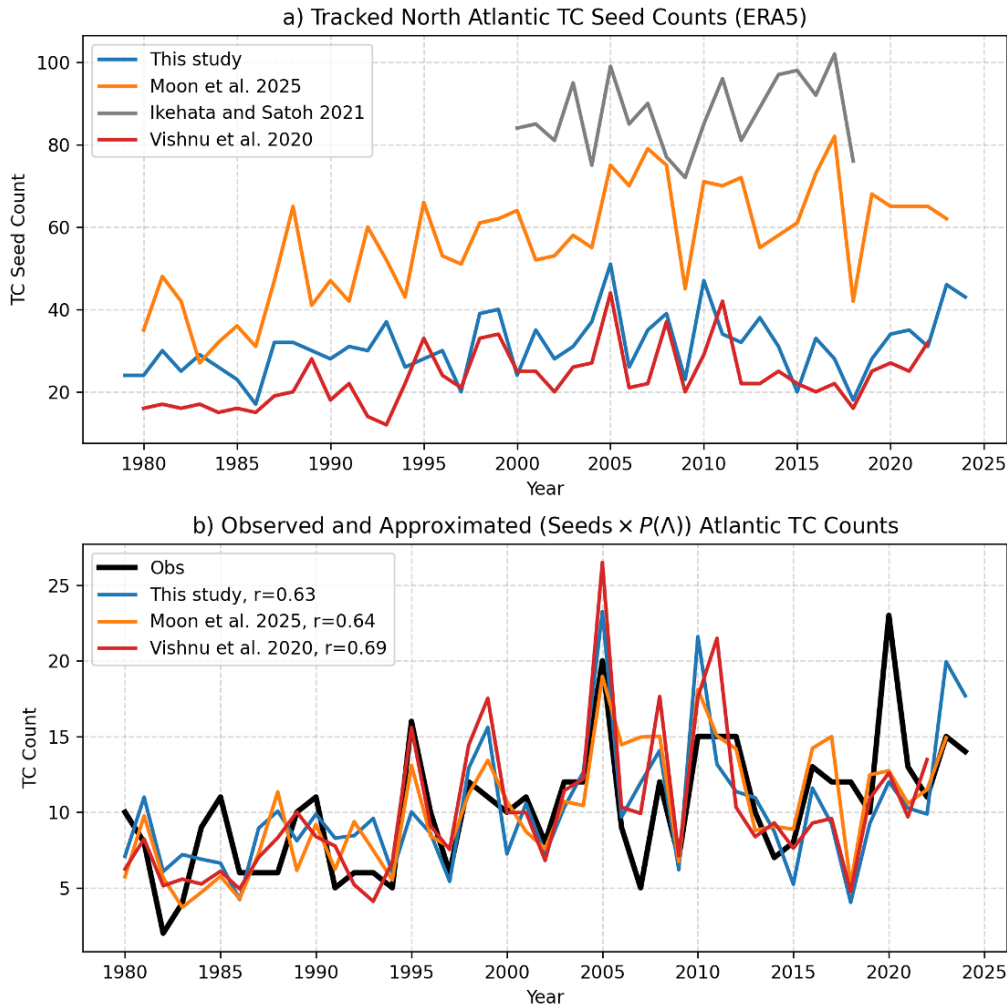


579 FIG. 5. Monthly mean products of  $SPI \times P(\Lambda)$  computed using four methodological approaches applied  
 580 to ERA5 data during the Atlantic tropical cyclone season (June–November) for (a) 2020, (b) 2010, and (c)  
 581 2005. The blue line corresponds to approach 1,  $SPI_{\text{Daily}} \times P(\Lambda)_{\text{Daily}}$ ; the orange line corresponds to approach  
 582 2,  $SPI_{\text{Monthly}} \times P(\Lambda)_{\text{Monthly}}$ ; the gray line corresponds to approach 3,  $SPI_{\text{Daily}} \times P(\Lambda)_{\text{Monthly}}$ ; and the red line  
 583 corresponds to approach 4,  $SPI_{\text{Monthly}} \times P(\Lambda)_{\text{Daily}}$ . The seasonal mean of the blue line, representing a proxy for  
 584 TC activity derived solely from daily data, is indicated by the horizontal blue dotted line. The seasonal mean  
 585 of the orange line, representing a proxy for TC activity derived solely from monthly data, is indicated by the  
 586 horizontal orange dotted line.

615 conditions, even this variability, as captured by the theoretical framework proposed by Hsieh et al.  
 616 (2020), cannot fully explain the realized activity.

#### 617 4. Discussion

618 This study examines the apparent unpredictability of the 2020 Atlantic TC season, during  
 619 which observed activity across all intensity bins, including TCs, hurricanes, and major hurricanes,  
 620 exceeded the ensemble spread of state-of-the-art GFDL atmosphere-only climate models forced  
 621 with observed SSTs (Fig. 1). Seasonal forecasts from both dynamical systems (Murakami et al.  
 622 2025) and DL-based models (Zhang et al. 2025a) similarly underestimated the realized storm  
 623 frequency across their ensemble spreads. Although Klotzbach et al. (2022) suggested that elevated



596 FIG. 6. (a) Tracked Atlantic tropical cyclone (TC) seed counts from the ERA5 dataset using the methods  
 597 described in Section 2 (blue; 1979–2024), from Moon et al. (2025) (orange; 1980–2023), Ikehata and Satoh  
 598 (2021) (gray; 2000–2018), and Vishnu et al. (2020) (red; 1980–2022). (b) Observed annual Atlantic TC counts  
 599 (black) and approximated annual TC frequencies derived from seed counts ( $\text{Seeds} \times P(\Lambda)$ ), where  $P(\Lambda)$  represents  
 600 the transition probability estimated from seasonally and MDR-averaged monthly ERA5 conditions. Seed counts  
 601 are obtained following the respective tracking methods in Section 2 (blue; 1980–2024), Moon et al. (2025)  
 602 (orange; 1980–2023), and Vishnu et al. (2020) (red; 1980–2022). Approximated TC counts are scaled by a  
 603 multiplicative factor so that their mean matches the observed mean. Correlation coefficients between observed  
 604 and approximated TC counts for each seed dataset are shown in the upper-left corner of panel (b).

624 late-season activity in 2020 may have been partially anticipated using large-scale indices, that work  
625 focused on intensity metrics such as Accumulated Cyclone Energy and rapid intensification. To  
626 the best of our knowledge, the predictability of storm frequency on seasonal timescales has not  
627 previously been examined.

628 We proposed two broad families of hypotheses to explain the discrepancy between observations  
629 and model simulations. The first considers whether model or observational deficiencies prevented  
630 the ensembles from capturing a hyperactive outcome comparable to that observed. The second  
631 examines whether the hyperactive season represented a dynamically plausible but low-probability  
632 outcome given the large-scale conditions present during the season.

633 After systematically testing four hypotheses within the first family using dynamical and statis-  
634 tical–dynamical models, we find little evidence supporting model or observational failure. Inde-  
635 pendent SST datasets yield consistent predictions of only moderately active conditions in 2020  
636 using a statistical-dynamical model (Fig. S1). Simulations forced with observed aerosols do  
637 not substantially increase activity relative to simulations using prescribed CMIP5 aerosols (Fig.  
638 S2). Idealized aerosol reduction experiments, acting as exaggerated analogues of the 2020 drop in  
639 aerosols) also show no statistically robust impact on basin-wide TC frequency (Fig. S3). Moreover,  
640 analysis of large-scale environmental conditions using the theoretical framework of Hsieh et al.  
641 (2020) indicates that 2020 did not exhibit environmental parameters strongly favoring a hyperactive  
642 season. Collectively, these results suggest that the SST-forced atmosphere-only models did not  
643 fundamentally fail in simulating moderate activity, as the large-scale state itself was not strongly  
644 conducive to a hyperactive TC season.

645 Using the theoretical framework, we further find that subseasonal variability in 2020 may have  
646 made it more difficult for the atmosphere-only GFDL models to simulate a hyperactive season  
647 given monthly boundary conditions alone (Fig. 4). In contrast, for other active seasons such as  
648 2005 and 2010, the same models produced relatively elevated activity under identical monthly SST  
649 forcing, suggesting that the character of intraseasonal atmospheric variability in 2020 reduced the  
650 likelihood of a hyperactive outcome within the ensemble. Even after incorporating known sources  
651 of subseasonal variability within the framework (Fig. 6), 2020 remains an outlier. This suggests  
652 the 2020 season was either a result of an exceptionally rare realization of internal atmospheric  
653 variability or from variability mechanisms not fully captured by the framework.

654 Additional features of the 2020 season are consistent with enhanced subseasonal noise. Activity  
655 was disproportionately concentrated in the Gulf of Mexico (Fig. S4), a region where TC variability  
656 is less tightly coupled to basin-scale predictors (Ng and Vecchi 2020). The season also included  
657 a large number of relatively weak storms compared with other hyperactive years such as 2005  
658 and 2010 (Fig. S5). These characteristics are consistent with a scenario in which weather-  
659 scale variability amplified seasonal counts beyond what would be anticipated from large-scale  
660 environmental forcing alone.

661 We also assessed whether 2020 can be interpreted as a low-probability outcome under the  
662 observed SST forcing by generating a 1,000-member ensemble of the year 2020 using the ACE2  
663 DL-based model. This large ensemble indicates that, under the observed 2020 SST forcing, a  
664 23-TC season corresponds to approximately a 0.5% event. Although such an outcome is highly  
665 unlikely in any single year, the probability of at least one 0.5% event occurring within a 45-year  
666 period is approximately 20%. Thus, the hyperactive 2020 season can be interpreted as a rare but  
667 dynamically plausible realization rather than clear evidence of systematic model failure.

## 668 **5. Conclusions**

669 The evidence presented here supports the conclusion that 2020 was a result of an unlikely  
670 atmospheric state, not necessarily a model or observational failure. Further, our results support the  
671 conclusion that the hyperactive 2020 season can be understood as an unlikely outcomes that even a  
672 well-calibrated system, like the modeling systems used in this study, will exhibit. This interpretation  
673 does not exclude the possibility that additional mechanisms not examined here contributed to the  
674 observed activity. Future observations, modeling advances, or reanalysis improvements could alter  
675 this assessment. New evidence could emerge to support hypotheses one through four, for which we  
676 were not able to find compelling support in the results presented here. Moreover, if similar large  
677 discrepancies between observations and model ensembles become more frequent, reassessment of  
678 model calibration and structural assumptions would be warranted.

679 Our findings have several broader implications. First, the 2020 season occurs at the end of  
680 the recent historical record and is anomalously hyperactive, which makes it disproportionately  
681 influential in linear trend estimates (Fig. S7). Because trend calculations are especially sensitive  
682 to extreme values near the endpoints of a time series, the inclusion of 2020 amplifies the estimated

683 1980–2024 increase in Atlantic TC, hurricane, and major hurricane activity by approximately 6  
684 storms per century for TCs, 2 storms per century for hurricanes, and 1 storm per century for  
685 major hurricanes. Although removing 2020 does not reverse the positive sign of the TC or major  
686 hurricane trends at the 95% confidence level, it substantially reduces their magnitudes. In contrast,  
687 for hurricanes, excluding 2020 causes the 95% confidence interval to cross zero, implying that the  
688 statistical evidence for a positive hurricane trend weakens considerably in its absence. This behavior  
689 indicates that 2020 acts as a high-leverage endpoint in the regression and exerts disproportionate  
690 influence on the inferred trends. This sensitivity is important because projected changes in TC  
691 frequency under anthropogenic forcing remain an open and actively debated research question  
692 (e.g., Knutson et al. 2020; Sobel et al. 2021). If the exceptional 2020 season primarily reflects  
693 internal variability, such as subseasonal fluctuations or weather-scale noise, then its strong influence  
694 on multidecadal trends complicates the interpretation of those trends as indicators of externally  
695 forced climate change. These results highlight the need for caution when drawing conclusions  
696 about long-term TC trends from relatively short observational records, particularly when extreme  
697 endpoint seasons exert substantial leverage on estimated changes. Our findings therefore stress the  
698 importance of employing statistical measures more resistant to the influence of outliers, such as  
699 the median of pairwise slopes (Lazante 1996).

700 Second, this study underscores the importance of properly characterizing ensemble uncertainty,  
701 especially with a limited ensemble size (e.g., Deser et al. 2012; Deser 2020; Deser and Phillips  
702 2023). Small ensemble sizes may underrepresent tail risk and can create the impression that  
703 out-of-range observations reflect model failure. Even with well-calibrated models, we still must  
704 plan for extreme departures from the ensemble mean, since they are still possible outcomes.

705 Third, our results underscore the important role of subseasonal variability and weather-scale  
706 noise in shaping seasonal TC outcomes. The analysis suggests that 2020 may have been more  
707 strongly influenced by subseasonal variability than other recent active seasons (Fig. 4). Such  
708 variability could reduce the ability of atmosphere-only models, when forced with monthly boundary  
709 conditions, to reproduce the observed level of hyperactivity. This finding reinforces the need to  
710 carefully separate externally forced climate signals from internally generated variability when  
711 interpreting extreme seasons. Weather-scale fluctuations can project onto seasonal statistics and  
712 thereby contaminate apparent climate signals (Kortum et al. 2024). Consequently, caution is

713 warranted when attributing an extreme season such as 2020 to long-term climate variability without  
714 explicitly accounting for the contribution of internal atmospheric noise.

715 Lastly, this study is one of many to highlight the value of very large ensembles (e.g., Mahesh  
716 et al. 2024a,b). We found that the five to ten member size from the dynamical models used in  
717 this study is not sufficient to study a full distribution of potential outcomes, especially given that  
718 the observed record is expected to exceed the ensemble spread across a multidecadal historical  
719 record several times. Traditional modeling efforts leverage a relatively small ensemble size. For  
720 example, the seasonal forecasting systems in Murakami et al. (2025) and Zhang et al. (2025a) use  
721 ensembles of 10–15 members, and operational global meteorological agencies generally use no  
722 more than a few dozen. In contrast, this study employs 1,000 ensemble members of the ACE2  
723 DL model to assess the full distribution of outcomes for 2020 Atlantic TC season. By leveraging  
724 the computational efficiency of DL-based weather and climate emulators, future forecast systems  
725 should continue to incorporate much larger ensembles and explicitly consider tail risks, rather than  
726 depending primarily on ensemble means, to prepare for low-probability but high-impact events.

727 In summary, the 2020 Atlantic TC season appears consistent with a rare realization within a  
728 probabilistic framework rather than a systemic model failure. Even well-calibrated forecasting  
729 systems will occasionally encounter extreme outcomes like the 2020 season. Recognizing and  
730 quantifying this possibility is essential for interpreting past extremes and preparing for future risk.

731 *Acknowledgments.* We thank Greg Hakim, Gabriele Villarini, Stephan Fueglistaler, Hiro Mu-  
732 rakami, Aidan Mahoney, and Gabe Rios for helpful discussion and comments, and we thank  
733 Spencer Clark at Ai2 and Colm Talbot and Mattie Niznik at Princeton Research Computing for  
734 their assistance in running the ACE2 model. We would like to thank Chanyoung Park for helping  
735 prepare the MERRRA-2 aerosol files in a format compatible with the models used in this study.  
736 This work has been supported by the Carbon Mitigation Initiative at Princeton University, funded  
737 by BP. E.L. was supported by the National Science Foundation Graduate Research Fellowship.  
738 This work was funded, in part, by the Heising-Simons Foundation Grant 2023-4720. The simula-  
739 tions were performed on computational resources managed and supported by Princeton Research  
740 Computing, a consortium of groups including the Princeton Institute for Computational Science  
741 and Engineering, the Office of Information Technology’s High Performance Computing Center,  
742 and the Visualization Laboratory at Princeton University.

743 *Data availability statement.* Source code of the HIRAM model is available from [https://](https://www.gfdl.noaa.gov/hiram-quickstart)  
744 [www.gfdl.noaa.gov/hiram-quickstart](https://www.gfdl.noaa.gov/hiram-quickstart), and the source code of the ACE2 model is available  
745 from <https://github.com/ai2cm/ace>. The forcing data and initial conditions for the ACE2  
746 model are available from [https://huggingface.co/allenai/ACE2-ERA5/tree/main/](https://huggingface.co/allenai/ACE2-ERA5/tree/main/initial_conditions)  
747 [initial\\_conditions](https://huggingface.co/allenai/ACE2-ERA5/tree/main/initial_conditions). ERA5 data are available from [https://cds.climate.copernicus.](https://cds.climate.copernicus.eu/datasets/reanalysis-era5-pressure-levels-monthly-means?tab=overview)  
748 [eu/datasets/reanalysis-era5-pressure-levels-monthly-means?tab=overview](https://cds.climate.copernicus.eu/datasets/reanalysis-era5-pressure-levels-monthly-means?tab=overview), and  
749 MERRA2 data are available from [https://gmao.gsfc.nasa.gov/gmao-products/](https://gmao.gsfc.nasa.gov/gmao-products/merra-2/data-access_merra-2/)  
750 [merra-2/data-access\\_merra-2/](https://gmao.gsfc.nasa.gov/gmao-products/merra-2/data-access_merra-2/). The OISST data are available from [https://www.ncei.](https://www.ncei.noaa.gov/products/optimum-interpolation-sst)  
751 [noaa.gov/products/optimum-interpolation-sst](https://www.ncei.noaa.gov/products/optimum-interpolation-sst), the HadISST data are available from  
752 <https://www.metoffice.gov.uk/hadobs/hadisst/>, and the ERSST data are available  
753 from <https://www.ncei.noaa.gov/products/extended-reconstructed-sst>. The code  
754 to compute the components of the tropical cyclone activity proxy are available from [https:](https://github.com/tlhsieh/tropical_cyclone_seeds)  
755 [//github.com/tlhsieh/tropical\\_cyclone\\_seeds](https://github.com/tlhsieh/tropical_cyclone_seeds) and [https://github.com/wy2136/](https://github.com/wy2136/wyhton/tree/main/xtci/shared)  
756 [wyhton/tree/main/xtci/shared](https://github.com/wy2136/wyhton/tree/main/xtci/shared). The TC seed dataset of Ikehata and Satoh (2021) is avail-  
757 able at <https://doi.org/10.5281/zenodo.5136292>, the low pressure system dataset of  
758 Vishnu et al. (2020) is available at [https://portal.nersc.gov/cfs/m3310/VishnuEtAl\\_](https://portal.nersc.gov/cfs/m3310/VishnuEtAl_TrackDataset/)  
759 [TrackDataset/](https://portal.nersc.gov/cfs/m3310/VishnuEtAl_TrackDataset/), and the seed dataset of Moon et al. (2025) is available at [https://doi.org/](https://doi.org/10.5281/zenodo.15227119)  
760 [10.5281/zenodo.15227119](https://doi.org/10.5281/zenodo.15227119). The code to run one year’s 1,000-member ensemble and process the

761 output, and track TCs is available at [https://github.com/emmalevin/ACE2\\_1000](https://github.com/emmalevin/ACE2_1000). TC track  
762 data and monthly mean environmental conditions generated from the ACE2 1,000 member ensem-  
763 ble are available at the Zenodo repository: <https://doi.org/10.5281/zenodo.19456833>.

## 764 **References**

765 Bi, K., L. Xie, H. Zhang, X. Chen, X. Gu, and Q. Tian, 2023: Accurate medium-range global  
766 weather forecasting with 3d neural networks. *Nature*, **619 (7970)**, 533–538, [https://doi.org/](https://doi.org/10.1038/s41586-023-06185-3)  
767 [10.1038/s41586-023-06185-3](https://doi.org/10.1038/s41586-023-06185-3).

768 Chan, D., G. A. Vecchi, W. Yang, and P. Huybers, 2021: Improved simulation of 19th- and 20th-  
769 century north atlantic hurricane frequency after correcting historical sea surface temperatures.  
770 *Science Advances*, **7 (26)**, eabg6931, <https://doi.org/10.1126/sciadv.abg6931>.

771 Chen, J.-H., and S.-J. Lin, 2011: The remarkable predictability of interannual variability of  
772 atlantic hurricanes during the past decade. *Geophysical Research Letters*, **38 (11)**, L11 804,  
773 <https://doi.org/10.1029/2011GL047629>.

774 Chen, L., X. Zhong, F. Zhang, Y. Cheng, Y. Xu, Y. Qi, and H. Li, 2023: Fuxi: A cascade machine  
775 learning forecasting system for 15-day global weather forecast. *npj Climate and Atmospheric*  
776 *Science*, **6 (1)**, 190, <https://doi.org/10.1038/s41612-023-00512-1>.

777 Chien, M.-T., E. A. Barnes, and E. D. Maloney, 2025: Modulation of tropical cyclogenesis  
778 on subseasonal-to-interannual timescales in the deep-learning climate emulator ace2. *Machine*  
779 *Learning: Earth*, **1 (1)**, 015 008, <https://doi.org/10.1088/3049-4753/adfd61>.

780 Delworth, T. L., and Coauthors, 2012: Simulated climate and climate change in the GFDL CM2.5  
781 high-resolution coupled climate model. *Journal of Climate*, **25 (8)**, 2755–2781, [https://doi.org/](https://doi.org/10.1175/JCLI-D-11-00316.1)  
782 [10.1175/JCLI-D-11-00316.1](https://doi.org/10.1175/JCLI-D-11-00316.1).

783 Deser, C., 2020: Certain uncertainty: The role of internal climate variability in projections  
784 of regional climate change and risk management. *Earth's Future*, **8 (12)**, e2020EF001854,  
785 <https://doi.org/10.1029/2020EF001854>.

- 786 Deser, C., A. Phillips, V. Bourdette, and H. Teng, 2012: Uncertainty in climate change projections:  
787 the role of internal variability. *Climate Dynamics*, **38** (3-4), 527–546, <https://doi.org/10.1007/s00382-010-0977-x>.  
788
- 789 Deser, C., and A. S. Phillips, 2023: A range of outcomes: the combined effects of internal variability  
790 and anthropogenic forcing on regional climate trends over europe. *Nonlinear Processes in*  
791 *Geophysics*, **30** (1), 63–84, <https://doi.org/10.5194/npg-30-63-2023>.
- 792 Diamond, M. S., 2023: Detection of large-scale cloud microphysical changes within a major  
793 shipping corridor after implementation of the international maritime organization 2020 fuel  
794 sulfur regulations. *Atmospheric Chemistry and Physics*, **23** (14), 8259–8269, <https://doi.org/10.5194/acp-23-8259-2023>.  
795
- 796 Eusebi, R., W. Yang, G. A. Vecchi, and S. Fueglistaler, 2025: Statistical modeling of north atlantic  
797 hurricane frequency and the impact and role of patterned warming. *Journal of Climate*, **38** (19),  
798 5391–5410, <https://doi.org/10.1175/JCLI-D-24-0647.1>.
- 799 Gelaro, R., and Coauthors, 2017: The modern-era retrospective analysis for research and ap-  
800 plications, version 2 (MERRA-2). *Journal of Climate*, **30** (14), 5419–5454, <https://doi.org/10.1175/JCLI-D-16-0758.1>.  
801
- 802 Gray, W. M., 1984: Atlantic seasonal hurricane frequency. part ii: Forecasting its variability.  
803 *Monthly Weather Review*, **112** (9), 1669–1683.
- 804 Hersbach, H., and Coauthors, 2020: The ERA5 global reanalysis. *Quarterly Journal of the Royal*  
805 *Meteorological Society*, **146** (730), 1999–2049, <https://doi.org/10.1002/qj.3803>.
- 806 Hsieh, T.-L., G. A. Vecchi, W. Yang, I. M. Held, and S. T. Garner, 2020: Large-scale control  
807 on the frequency of tropical cyclones and seeds: a consistent relationship across a hierarchy  
808 of global atmospheric models. *Climate Dynamics*, **55** (11), 3177–3196, <https://doi.org/10.1007/s00382-020-05446-5>.  
809
- 810 Huang, B., C. Liu, V. Banzon, E. Freeman, G. Graham, B. Hankins, T. Smith, and H.-M. Zhang,  
811 2021: Improvements of the daily optimum interpolation sea surface temperature (doisst) version  
812 2.1. *Journal of Climate*, **34** (8), 2923–2939, <https://doi.org/10.1175/JCLI-D-20-0166.1>.

813 Huang, B., and Coauthors, 2017: Extended reconstructed sea surface temperature, version 5  
814 (ersstv5): Upgrades, validations, and intercomparisons. *Journal of Climate*, **30** (20), 8179–  
815 8205, <https://doi.org/10.1175/JCLI-D-16-0836.1>.

816 Ikehata, K., and M. Satoh, 2021: Climatology of tropical cyclone seed frequency and survival rate  
817 in tropical cyclones. *Geophysical Research Letters*, **48** (18), e2021GL093626, <https://doi.org/10.1029/2021GL093626>.  
818

819 Jordan, G., and M. Henry, 2024: IMO2020 regulations accelerate global warming by up to 3 years  
820 in UKESM1. *Earth's Future*, **12** (8), e2024EF005011, <https://doi.org/10.1029/2024EF005011>.

821 Klotzbach, P. J., S. G. Bowen, R. Pielke, and M. Bell, 2018: Continental u.s. hurricane landfall  
822 frequency and associated damage: Observations and future risks. *Bulletin of the American  
823 Meteorological Society*, **99** (7), 1359–1376, <https://doi.org/10.1175/BAMS-D-17-0184.1>.

824 Klotzbach, P. J., and W. M. Gray, 2003: Forecasting september atlantic basin tropical cyclone  
825 activity. *Weather and Forecasting*, **18** (6), 1109–1128, [https://doi.org/10.1175/1520-0434\(2003\)  
826 018<1109:FSABTC>2.0.CO;2](https://doi.org/10.1175/1520-0434(2003)018<1109:FSABTC>2.0.CO;2).

827 Klotzbach, P. J., and Coauthors, 2022: A hyperactive end to the atlantic hurricane season oc-  
828 tober–november 2020. *Bulletin of the American Meteorological Society*, **103** (1), S1–S28,  
829 <https://doi.org/10.1175/BAMS-D-20-0312.1>.

830 Knutson, T., and Coauthors, 2020: Tropical cyclones and climate change assessment: Part II:  
831 Projected response to anthropogenic warming. **101** (3), E303–E322, [https://doi.org/10.1175/  
832 BAMS-D-18-0194.1](https://doi.org/10.1175/BAMS-D-18-0194.1).

833 Kochkov, D., and Coauthors, 2024: Neural general circulation models for weather and climate.  
834 *Nature*, **632** (8027), 1060–1066, <https://doi.org/10.1038/s41586-024-07744-y>.

835 Kortum, G., G. A. Vecchi, T.-L. Hsieh, and W. Yang, 2024: Influence of weather and climate  
836 on multidecadal trends in atlantic hurricane genesis and tracks. *Journal of Climate*, **37** (5),  
837 1501–1522, <https://doi.org/10.1175/JCLI-D-23-0088.1>.

838 Lam, R., and Coauthors, 2023: Learning skillful medium-range global weather forecasting. *Sci-  
839 ence*, **382** (6677), 1416–1421, <https://doi.org/10.1126/science.adi2336>.

840 Landsea, C. W., G. A. Vecchi, L. Bengtsson, and T. R. Knutson, 2010: Impact of duration thresholds  
841 on atlantic tropical cyclone counts. **23 (10)**, 2508–2519, <https://doi.org/10.1175/2009JCLI3034>.  
842 1.

843 Lang, S., and Coauthors, 2024: AIFS: ECMWF’s data-driven forecasting system. URL <https://arxiv.org/abs/2406.01465>, arXiv preprint, <https://doi.org/10.48550/arXiv.2406.01465>, 2406.  
844 <https://doi.org/10.48550/arXiv.2406.01465>, 2406.  
845 01465.

846 Lazante, J. R., 1996: Resistant, robust and non-parametric techniques for the analysis of  
847 climate data: Theory and examples, including applications to historical radiosonde sta-  
848 tion data. **16 (11)**, 1197–1226, [https://doi.org/10.1002/\(SICI\)1097-0088\(199611\)16:11<1197::](https://doi.org/10.1002/(SICI)1097-0088(199611)16:11<1197::AID-JOC89>3.0.CO;2-L)  
849 [AID-JOC89\)3.0.CO;2-L](https://doi.org/10.1002/(SICI)1097-0088(199611)16:11<1197::AID-JOC89>3.0.CO;2-L).

850 Levin, E. L., G. A. Vecchi, and W. Yang, 2025: Influence of sea surface temperature patterns  
851 and mean warming on past and future atlantic hurricane activity. *EarthArXiv preprint Earth-*  
852 *ArXiv:10.31223/X5FX8S*, <https://doi.org/10.31223/X5FX8S>.

853 Mahesh, A., and Coauthors, 2024a: Huge ensembles part i: Design of ensemble weather forecasts  
854 using spherical fourier neural operators. *arXiv preprint arXiv:2408.03100*, [https://doi.org/10.](https://doi.org/10.48550/arXiv.2408.03100)  
855 [48550/arXiv.2408.03100](https://doi.org/10.48550/arXiv.2408.03100).

856 Mahesh, A., and Coauthors, 2024b: Huge ensembles part ii: Properties of a huge ensemble of  
857 hindcasts generated with spherical fourier neural operators. *arXiv preprint arXiv:2408.01581*,  
858 <https://doi.org/10.48550/arXiv.2408.01581>.

859 Menemenlis, S., G. A. Vecchi, W. Yang, S. Fueglistaler, and S. P. Raghuraman, 2025: Consequential  
860 differences in satellite-era sea surface temperature trends across datasets. *Nature Climate Change*,  
861 **15 (8)**, 897–903, <https://doi.org/10.1038/s41558-025-02362-6>.

862 Moon, J., D. Kim, A. A. Wing, S. J. Camargo, G. N. Emlaw, J. C. Starr, and D.-H. Cha, 2025: Trop-  
863 ical cyclone seed disturbances in ERA5. *Journal of Climate*, **38 (18)**, 4625–4639, [https://doi.org/](https://doi.org/10.1175/JCLI-D-24-0291.1)  
864 [10.1175/JCLI-D-24-0291.1](https://doi.org/10.1175/JCLI-D-24-0291.1).

865 Murakami, H., 2022: Substantial global influence of anthropogenic aerosols on tropical cyclones  
866 over the past 40 years. *Science Advances*, **8 (19)**, eabn9493, [https://doi.org/10.1126/sciadv.](https://doi.org/10.1126/sciadv.abn9493)  
867 [abn9493](https://doi.org/10.1126/sciadv.abn9493).

- 868 Murakami, H., 2024: Effect of regional anthropogenic aerosols on tropical cyclone frequency of  
869 occurrence. *Geophysical Research Letters*, **51 (21)**, e2024GL110443, [https://doi.org/10.1029/](https://doi.org/10.1029/2024GL110443)  
870 2024GL110443.
- 871 Murakami, H., T. L. Delworth, N. C. Johnson, F. Lu, C. E. McHugh, and L. Jia, 2025: Seasonal  
872 forecasts of tropical cyclones using GFDL SPEAR and HiFLOR-s. *Journal of Climate*, **38 (9)**,  
873 3601–3620, <https://doi.org/10.1175/JCLI-D-24-0356.1>.
- 874 Ng, C. H. J., and G. A. Vecchi, 2020: Large-scale environmental controls on the seasonal statistics  
875 of rapidly intensifying north atlantic tropical cyclones. *Climate Dynamics*, **54 (9-10)**, 3907–3925,  
876 <https://doi.org/10.1007/s00382-020-05207-4>.
- 877 Pielke, R. A., J. Gratz, C. W. Landsea, D. Collins, M. A. Saunders, and R. Musulin, 2008:  
878 Normalized hurricane damage in the united states: 1900–2005. **9 (1)**, 29–42, [https://doi.org/](https://doi.org/10.1061/(ASCE)1527-6988(2008)9:1(29))  
879 10.1061/(ASCE)1527-6988(2008)9:1(29).
- 880 Schneider, D. P., C. Deser, J. Fasullo, and K. E. Trenberth, 2013: Climate data guide spurs  
881 discovery and understanding. *Eos, Transactions American Geophysical Union*, **94 (13)**, 121–  
882 122, <https://doi.org/10.1002/2013EO130001>.
- 883 Sobel, A. H., A. A. Wing, S. J. Camargo, C. M. Patricola, G. A. Vecchi, C. Lee, and M. K. Tippett,  
884 2021: Tropical cyclone frequency. *Earth's Future*, **9 (12)**, e2021EF002275, [https://doi.org/](https://doi.org/10.1029/2021EF002275)  
885 10.1029/2021EF002275.
- 886 Tang, B., and K. Emanuel, 2010: Midlevel ventilation's constraint on tropical cyclone intensity.  
887 *Journal of the Atmospheric Sciences*, **67 (6)**, 1817-1830, <https://doi.org/10.1175/2010JAS3318>.  
888 1.
- 889 Tang, B., and K. Emanuel, 2012: A ventilation index for tropical cyclones. *Bulletin of the American*  
890 *Meteorological Society*, **93 (12)**, 1901-1915, <https://doi.org/10.1175/BAMSD1100165.1>.
- 891 Ullrich, P. A., and C. M. Zarzycki, 2017: TempestExtremes: a framework for scale-insensitive  
892 pointwise feature tracking on unstructured grids. *Geoscientific Model Development*, **10 (3)**,  
893 1069–1090, <https://doi.org/10.5194/gmd-10-1069-2017>.

- 894 Vecchi, G. A., and B. J. Soden, 2007: Effect of remote sea surface temperature change on  
895 tropical cyclone potential intensity. *Nature*, **450 (7172)**, 1066–1070, [https://doi.org/10.1038/](https://doi.org/10.1038/nature06423)  
896 [nature06423](https://doi.org/10.1038/nature06423).
- 897 Vecchi, G. A., and G. Villarini, 2014: Next season’s hurricanes. *Science*, **343 (6171)**, 618–619,  
898 <https://doi.org/10.1126/science.1247759>.
- 899 Vecchi, G. A., M. Zhao, H. Wang, G. Villarini, A. Rosati, A. Kumar, I. M. Held, and R. Gudgel,  
900 2011: Statistical–dynamical predictions of seasonal north atlantic hurricane activity. *Monthly*  
901 *Weather Review*, **139 (4)**, 1071–1087, <https://doi.org/10.1175/2010MWR3499.1>.
- 902 Vecchi, G. A., and Coauthors, 2014: On the seasonal forecasting of regional tropical cyclone  
903 activity. <https://doi.org/10.1175/JCLI-D-14-00158.1>.
- 904 Vecchi, G. A., and Coauthors, 2019: Tropical cyclone sensitivities to co2 doubling: roles of  
905 atmospheric resolution, synoptic variability and background climate changes. *Climate Dynamics*,  
906 **53 (9)**, 5999–6033, <https://doi.org/10.1007/s00382-019-04913-y>.
- 907 Villarini, G., G. A. Vecchi, T. R. Knutson, M. Zhao, and J. A. Smith, 2011: North atlantic tropical  
908 storm frequency response to anthropogenic forcing: Projections and sources of uncertainty.  
909 *Journal of Climate*, **24 (13)**, 3224–3248, <https://doi.org/10.1175/2011JCLI3853.1>.
- 910 Vishnu, S., W. R. Boos, P. A. Ullrich, and T. A. O’Brien, 2020: Assessing historical variability  
911 of south asian monsoon lows and depressions with an optimized tracking algorithm. *Journal*  
912 *of Geophysical Research: Atmospheres*, **125 (15)**, e2020JD032977, [https://doi.org/10.1029/](https://doi.org/10.1029/2020JD032977)  
913 [2020JD032977](https://doi.org/10.1029/2020JD032977).
- 914 Vitart, F., and T. N. Stockdale, 2001: Seasonal forecasting of tropical storms using cou-  
915 pled gcm integrations. *Monthly Weather Review*, **129 (10)**, 2521–2537, [https://doi.org/](https://doi.org/10.1175/1520-0493(2001)129<2521:SFOTSU>2.0.CO;2)  
916 [10.1175/1520-0493\(2001\)129<2521:SFOTSU>2.0.CO;2](https://doi.org/10.1175/1520-0493(2001)129<2521:SFOTSU>2.0.CO;2).
- 917 Watt-Meyer, O., and Coauthors, 2025: ACE2: Accurately learning subseasonal to decadal at-  
918 mospheric variability and forced responses. *npj Climate and Atmospheric Science*, **8 (1)**, 205,  
919 <https://doi.org/10.1038/s41612-025-01090-0>.

- 920 Weinkle, J., C. Landsea, D. Collins, R. Musulin, R. P. Crompton, P. J. Klotzbach, and R. Pielke,  
921 2018: Normalized hurricane damage in the continental united states 1900–2017. *Nature Sus-*  
922 *tainability*, **1 (12)**, 808–813, <https://doi.org/10.1038/s41893-018-0165-2>.
- 923 Yang, W., T.-L. Hsieh, and G. A. Vecchi, 2021: Hurricane annual cycle controlled by both seeds and  
924 genesis probability. *Proceedings of the National Academy of Sciences*, **118 (41)**, e2108397 118,  
925 <https://doi.org/10.1073/pnas.2108397118>.
- 926 Young, R., and S. Hsiang, 2024: Mortality caused by tropical cyclones in the united states. *Nature*,  
927 **635 (8037)**, 121–128, <https://doi.org/10.1038/s41586-024-07945-5>.
- 928 Zhang, G., M. Rao, J. Yuval, and M. Zhao, 2025a: Advancing seasonal prediction of tropical  
929 cyclone activity with a hybrid ai–physics climate model. *Environmental Research Letters*, **20 (9)**,  
930 094 031, <https://doi.org/10.1088/1748-9326/adf864>.
- 931 Zhang, J., Y.-S. Chen, E. Gryspeerdt, T. Yamaguchi, and G. Feingold, 2025b: Radiative forcing  
932 from the 2020 shipping fuel regulation is large but hard to detect. *Communications Earth &*  
933 *Environment*, **6 (1)**, 1–11, <https://doi.org/10.1038/s43247-024-01911-9>.
- 934 Zhao, M., and I. M. Held, 2010: An analysis of the effect of global warming on the intensity  
935 of atlantic hurricanes using a gcm with statistical refinement. *Journal of Climate*, **23 (23)**,  
936 6382–6395, <https://doi.org/10.1175/2010JCLI3837.1>.
- 937 Zhao, M., I. M. Held, S.-J. Lin, and G. A. Vecchi, 2009: Simulations of global hurricane clima-  
938 tology, interannual variability, and response to global warming using a 50-km resolution gcm.  
939 *Journal of Climate*, **22 (24)**, 6653–6678, <https://doi.org/10.1175/2009JCLI3049.1>.
- 940 Zhao, M., I. M. Held, and G. A. Vecchi, 2010: Retrospective forecasts of the hurricane season using  
941 a global atmospheric model assuming persistence of sst anomalies. *Monthly Weather Review*,  
942 **138 (10)**, 3858–3868, <https://doi.org/10.1175/2010MWR3366.1>.